A Unified Theory of Electro-Magnetic-Gravitational-Acceleration Force Density Interactions for Stable Nuclear Fusion

A Novel Theoretical Framework

Wim Vegt
Department of Physics
Eindhoven University of Technology
The Netherlands
wimvegt@quantumlight.science

Abstract

Nuclear fusion represents a frontier melding the realms of material science, typified by fusion fuels like Deuterium, and energy science, characterized by microwave heating methodologies. Current theoretical physics paradigms fall short in adequately describing the complex interactions required to stabilize nuclear fusion, particularly within confinement devices such as Tokamaks. Addressing this limitation necessitates a novel theory that accurately encompasses the interactions between electro-magnetic-gravitational force densities (expressed in N/m^3) and their mechanical analogues, articulated through the Navier-Stokes equation for compressible nuclear plasmas.

This pioneering theoretical framework offers an all-encompassing perspective on electro-magnetic-gravitational-acceleration force density interactions across both astronomical and subatomic scales. It spans phenomena as diverse as Gravitational RedShift, Black Holes, and the discrete energy levels of atomic light absorption and emission. Uniquely, this theory integrates electrodynamics and plasma dynamics into a single cohesive model. Traditionally overlooked, gravitational (acceleration) forces resulting from rotational and linear accelerations are revealed here as pivotal for achieving stable nuclear fusion.

Unlike General Relativity, this new theory is grounded on the combined divergence of the “Stress-Energy Tensor” and the “Gravitational-Acceleration” Tensor. It elucidates "Gravitational-Acceleration-Electromagnetic" interactions, providing mathematical tensor solutions for Black Holes or Gravitational Electromagnetic Confinements. The "Electromagnetic Energy Gradient" generates a second-order "Lorentz

Transformation," translating into the Gravitational Field of Black Holes, which dictates force density interactions between light confinement and the “Gravitational-Acceleration” Field.

In juxtaposition to Einstein's introduction of the "Einstein Gravitational Constant" within the four-dimensional Energy-Stress Tensor, our theory capitalizes on the additive properties of the Electromagnetic Tensor and the “Gravitational-Acceleration” Tensor. This revised vantage point unveils the concept of "CURL" within gravitational fields surrounding Black Holes, influencing Gravitational Lensing—phenomena unaccounted for by General Relativity.

Additionally, the theory identifies "Electromagnetic-Gravitational Interaction," "Magnetic-Gravitational Interaction," and "Electric-Gravitational Interaction." It proposes that interactions are exclusive to field interactions rather than particle-field interactions as traditionally conceived: electric fields engage with other electric fields, magnetic fields with other magnetic fields, and gravitational fields with other gravitational fields.

This advanced theoretical approach provides precise mathematical descriptions of Black Holes, as initially proposed by John Archibald Wheeler in 1955. The theoretical solutions for Black Holes are integral to the Dirac equation's tensor form in relativistic quantum mechanics. Assuming a constant speed of light (c) and Planck’s constant within a Black Hole, the radius of a Black Hole with the energy of a proton approximates 1% of a hydrogen atom radius.

Empirical substantiation is derived from experiments involving two Galileo satellites and a Ground Station, where Gravitational RedShift was measured using a stable MASER frequency. The discrepancy between General Relativity and the New Theory's predictions for Gravitational RedShift within Earth's gravitational field is less than 10^(-16). Observational data since W.S. Adams' 1925 measurement of the gravitational redshift in the spectral lines from the White Dwarf companion to Sirius consistently aligns with both theories within negligible margins.

Theories seeking to unify Quantum Physics with General Relativity, such as "String Theory," suggest temporal variability in natural constants. However, precise observations from NASA’s Messenger mission have significantly constrained potential variations in the gravitational constant (G). A distinguishing feature of the New Theory is its prediction of a temporally constant (G), reinforcing the unification of General Relativity and Quantum Physics.

Keywords

Quantum Physics, General Relativity, Gravitational RedShift, Black Holes, Dark Matter, Nuclear Fusion, Nuclear Plasmas.

1. Introduction

Einstein approached the interaction between gravity and light by introducing the "Einstein Gravitational Constant" in the 4-dimensional Energy-Stress Tensor. However, in advancing our understanding of nuclear fusion processes, it becomes imperative to explore alternative frameworks that address gravitational and acceleration interactions more holistically.

1.1 Electromagnetic-Gravitational and Magnetic-Gravitational Interactions

This new theoretical approach eliminates the conventional particle-field interaction concept. Instead, it focuses on field-field interactions. According to this theory, particles do not interact directly with fields. Rather, the interaction between a charged particle and an electric field is reconceptualized as the interaction between the particle's own electric field and the external electric field. Similarly, magnetic fields interact directly with other magnetic fields, and gravitational fields interact with other gravitational fields.

By grounding every type of interaction—whether electromagnetic or gravitational—in field-field dynamics, this theory aligns with the principles of general relativity and relativistic quantum mechanics, ensuring a consistent and comprehensive depiction of complex inter-field processes. This approach has profound implications for the stability and efficiency of nuclear fusion reactors, such as Tokamaks, which depend on finely tuned electromagnetic and gravitational interactions to sustain high-energy plasmas.

1.2 Field-Field Interaction Implications for Nuclear Fusion

The implications of this theory for nuclear fusion are transformative. In traditional fusion models, the stability of plasma confinement within reactors like tokamaks is limited by our understanding of particle interactions with fields. By shifting to a field-field interaction paradigm, we gain deeper insights into the conditions necessary for maintaining stable plasma states, potentially overcoming barriers that have historically hindered the attainment of sustainable fusion energy.

1.3 The Role of Gravitational Fields

Gravitational interactions, particularly those arising from rotational and linear accelerations, play a crucial role in these processes. In the context of this new

theory, addressing the gravitational field components accurately becomes essential for refining plasma confinement techniques and advancing reactor designs. By incorporating gravitational fields into the interaction models, we can better predict and manage the dynamic behaviours of fusion plasmas, bridging gaps between theoretical predictions and experimental outcomes.

This alternative framework, which emphasizes field-field interactions over particle-field dynamics and integrates gravitational forces into the equation, presents a robust and unified approach for advancing nuclear fusion technology. It not only aligns with but also extends the existing paradigms of general relativity and relativistic quantum physics, offering promising pathways to overcome current limitations and achieve stable and efficient nuclear fusion.

2.1 Theoretical Framework for Nuclear Fusion

Einstein approached the interaction between gravity and light by the introduction of the "Einstein Gravitational Constant" in the 4-dimensional Energy-Stress Tensor.

$$G_{\mu\nu} + \Lambda\, g_{\mu\nu} = \kappa\, T_{\mu\nu} \tag{1}$$

In which $G_{\mu\nu}$ equals the Einstein Tensor, $g_{\mu\nu}$ equals the Metric Tensor, $T_{\mu\nu}$ equals the Stress-Energy tensor, Λ equals the cosmological constant and κ equals the Einstein gravitational constant.

An alternative approach to Einstein's expression with the tensor $\kappa T_{\mu\nu}$, describing the curvature of the Space-Time continuum, is the sum of the Electromagnetic Tensor $T_{\mu\nu}$ and the "Gravitational-Acceleration" Tensor $J_{\mu\nu}$.

$$\kappa\, T_{\mu\nu} \Leftrightarrow T_{\mu\nu} + J_{\mu\nu} \tag{2}$$

The 4-dimensional divergence of the sum of the Electromagnetic Stress-Energy tensor and the Gravitational Tensor expresses the 4-dimensional Force-Density vector (expressed in $[N/m^3]$ in the 3 spatial coordinates) as the result of Electro-Magnetic-Gravitational interaction.

$$f^{\mu} = \partial_{\nu}\left(T^{\mu\nu} + J^{\mu\nu}\right) \tag{3}$$

In vector notation the 4-dimensional Force-Density vector can be written as:

$$\overline{f}^{4} = \begin{pmatrix} f_4 \\ f_3 \\ f_2 \\ f_1 \end{pmatrix} = \square \bullet \left(\overline{\overline{T}} + \overline{\overline{J}}\right) \tag{4}$$

The fundamental boundary condition for this alternative approach to gravity is the requirement that the Force 4 vector equals zero in the 4 dimensions, expressing a universal 4-dimensional equilibrium:

$$\bar{f}^4 = \begin{pmatrix} f_4 \\ f_3 \\ f_2 \\ f_1 \end{pmatrix} = \square \bullet \left(\bar{\bar{T}} + \bar{\bar{J}} \right) = \bar{0}^4 \qquad (5)$$

The 3 spatial components of the Force-Density vector, as a result of Electro-Magnetic-Gravitational interaction can be written as:

$$\bar{f} = -\frac{1}{c^2}\frac{\partial (\bar{E} \times \bar{H})}{\partial t} + \varepsilon_0 \bar{E} (\nabla . \bar{E}) - \varepsilon_0 \bar{E} \times (\nabla \times \bar{E}) +$$

$$+ \mu_0 \bar{H} (\nabla . \bar{H}) - \mu_0 \bar{H} \times (\nabla \times \bar{H}) + \gamma_0 \bar{g} (\nabla . \bar{g}) - \gamma_0 \bar{g} \times (\nabla \times \bar{g}) = \bar{0} \quad [N/m^3]$$

in which:

$\varepsilon_0 (\nabla . \bar{E}) = \rho_E$ Electric Charge Density [C/ m^3]

$\mu_0 (\nabla . \bar{H}) = \rho_M$ Magnetic Flux Density [Vs/ m^3] or [Wb/ m^3]

$\gamma_0 (\nabla . \bar{g}) = \rho_M$ Mass Density (Electromagnetic) [kg/ m^3]

(6)

Electric Energy Density: $w_E = \frac{1}{2} \varepsilon_0 E^2$

Magnetic Energy Density: $w_M = \frac{1}{2} \mu_0 H^2$

Gravitational Energy Density: $w_G = \frac{1}{2} \gamma_0 g^2$

$\bar{g} \triangleq$ acceleration (gravitational or mechanical/dynamical)

In which E represents the electric field intensity expressed in [V/m], H represents the magnetic field intensity expressed in [A/m] and g represents the gravitational acceleration expressed in [m/s^2]. The permittivity indicated as ε_0, the permeability indicated as μ_0 and the gravitational permeability of vacuum as γ_0.

For curl-free gravitational fields equation (6) can be written as:

$$\bar{f} = -\frac{1}{c^2}\frac{\partial (\bar{E} \times \bar{H})}{\partial t} + \varepsilon_0 \bar{E} (\nabla . \bar{E}) - \varepsilon_0 \bar{E} \times (\nabla \times \bar{E}) +$$

$$+ \mu_0 \bar{H} (\nabla . \bar{H}) - \mu_0 \bar{H} \times (\nabla \times \bar{H}) + \bar{g} \rho_M = \bar{0} \quad [N/m^3] \qquad (7)$$

Substituting Einstein's $W = m c^2$ in (7) results in "Electro-Magnetic-Gravitational Equilibrium Field Equation" (8):

$$\bar{f} = -\frac{1}{c^2}\frac{\partial (\bar{E} \times \bar{H})}{\partial t} + \varepsilon_0 \bar{E} (\nabla . \bar{E}) - \varepsilon_0 \bar{E} \times (\nabla \times \bar{E}) + \quad (8)$$

$$+\mu_0 \bar{H} (\nabla . \bar{H}) - \mu_0 \bar{H} \times (\nabla \times \bar{H}) + \frac{1}{2c^2}\bar{g}\left(\varepsilon E^2 + \mu H^2\right) = \bar{0} \quad [N/m^3]$$

2.2 Field-Field Interaction Dynamics

In this advanced theoretical framework, all interactions are conceptualized as interactions between fields:

- **Electric fields interact with other electric fields.**
- **Magnetic fields interact with other magnetic fields.**
- **Gravitational fields interact with other gravitational fields.**

This paradigm shift emphasizes that interactions are mediated exclusively by the fields themselves, rather than direct particle-field interactions. Such a perspective yields a more integrated and coherent understanding of force interactions across both macroscopic and microscopic scales.

Implications for Advanced Physics and Nuclear Fusion

This paradigm significantly deepens our comprehension of fundamental forces, seamlessly extending the principles enshrined in general relativity and quantum field theory. By centring on field-field interactions, this theory illuminates novel insights into the stability and dynamics of plasma in nuclear fusion contexts. It enhances the theoretical foundations necessary for the development of more efficient and stable fusion reactors. Ultimately, this approach seeks to bridge existing gaps in our understanding, thereby paving the way for future advancements in nuclear fusion technology.

2.1 Verification of the New Theory Through Gravitational Redshift Experiment

To empirically validate the propositions set forth by the New Theory, a pivotal experiment known as the "Test of the Gravitational Redshift with Galileo Satellites in

an Eccentric Orbit" conducted by S. Hermann and collaborators has been selected for scrutiny. In this experimental setup:

A stable "MASER" frequency originating from a ground station is emitted to two Galileo Satellites positioned in orbit. The primary objective of this experiment is to measure the frequency differential effect observed between the Ground Station and the Satellites. Notably, the frequency shift is attributed to the gravitational influence exerted by the Earth, necessitating the utilization of two satellites to counterbalance the eccentricity inherent in the Galileo Orbit.

Upon assuming a gravitational field denoted as g[z], contingent upon the radial direction within the Cartesian coordinate system spanning the expanse from the ground station to the satellites:

$$\overline{g[z]} = \left\{0,0, \frac{G\, M_{Earth}}{4\, \pi\, z^2}\right\} \tag{9}$$

In which G ($G = 6.67428\ 10^{-11}\ Nm^2 / kg^2$) equals the Gravitational constant, M_{Earth} the mass of the earth and r the radial distance from the centre of the earth. The mathematical solution [5] of equation (8) for plane electromagnetic waves (expressed in cartesian {x,y,z} coordinates) related to the Electric Field Intensity equals:

The mathematical resolution for plane electromagnetic waves expressed in Cartesian coordinates {x, y, z}, deriving from equation (8) and within the context of G = 6.67428 x 10^-11 Nm^2 / kg^2 signifying the Gravitational constant, MEarth representing Earth's mass, and r denoting the radial distance from Earth's center, reveals the Electric Field Intensity to be:

$$\overline{E} = \begin{pmatrix} E_x \\ E_y \\ E_z \end{pmatrix} = \begin{pmatrix} e^{-\frac{G\, M_{Eearth}\ \varepsilon_0\ \mu_0}{8\, \pi\, z}}\ h\left[\ \omega_0\ e^{-\frac{G\, M_{Earth}\ \varepsilon_0\ \mu_0}{4\, \pi\, z}}\left(t - \sqrt{\varepsilon\ \mu}\ z\right)\ \right] \\ 0 \\ 0 \end{pmatrix} \tag{10}$$

And the mathematical solution of (8) for the Magnetic Field Intensity equals:

$$\overline{H} = \begin{pmatrix} H_x \\ H_y \\ H_z \end{pmatrix} = \begin{pmatrix} 0 \\ \frac{1}{\sqrt{\varepsilon_0\,\mu_0}}\, e^{-\frac{G\,M_{Earth}\,\varepsilon_0\,\mu_0}{8\,\pi\,z}}\, h\left[\omega_0\, e^{-\frac{G\,M_{Earth}\,\varepsilon_0\,\mu_0}{4\,\pi\,z}}\left(t - \sqrt{\varepsilon\,\mu}\,z\right)\right] \\ 0 \end{pmatrix} \tag{11}$$

In which In this scenario, ω_0 represents the initial frequency of the MASER radiation as it propagates along the gravitational field (g[z]) of the Earth in the z-direction. The exponential term elucidates the phenomenon of Gravitational Redshift occurring when the MASER radiation moves in alignment with Earth's gravitational field. Although the propagation speed of Electromagnetic Radiation remains constant - equivalent to the speed of light - the amplitude and frequency of the field intensity exhibit an exponential decay.

Through meticulous calculations performed in Mathematica, a consequential disparity emerges between the outcomes obtained through General Relativity and those via the New Theory. Specifically, with the ground station placed at a distance of (z_1 = 6,378,000) [m] (representing the Earth's radius) and the ESA satellites orbiting at an average distance of (z_2 = 23,222,000) [m] from the centre of the Earth, as computed through Mathematica, the Gravitational Redshift in accordance with General Relativity is determined as:

$$\Delta\,\omega_{GR} = 0.00000000004011815497097883\ [s^{-1}] \tag{12}$$

Calculated with Mathematica, the Gravitational RedShift according the New Theory, which is a solution of equation (8) equals:

$$\Delta\,\omega_{GR} = 0.00000000004011824206173742\ [s^{-1}] \tag{13}$$

Both calculated values a within the Range of the measured gravitational RedShift by the average values of both ESA satellites in the Galileo orbit

$$\Delta\,\omega_{\text{Measured}} = 0.000000000040118 \pm 2.2\,10^{-15}\ [s^{-1}] \tag{14}$$

In [2] a factor α has been defined which presents the measured deviation α between the predicted Gravitational RedShift by General Relativity and the Measured Gravitational RedShift.

$$\alpha = \Delta\,\omega_{\text{MEASURED}} - \Delta\,\omega_{GR} = (2.2 \pm 1.6) \times 10^{-5} \tag{15}$$

A comparable factor α can be used to determine which theory (General Relativity or the New Theory) has the nearest approach to the experimentally measured data. Highly accurate measuring experiments are required with an accuracy higher than 16 digits beyond the decimal point.

3 Black Holes

3.1 Black Holes without Singularities: Size Comparable to Hydrogen Atom Diameter

In a significant breakthrough, a secondary key solution emanating from equation (8) delineates a phenomenon termed Gravitational Electromagnetic Confinement, commonly recognized as a BLACK HOLE. This scenario unfolds within a radial gravitational field boasting acceleration in the radial direction. Notably, this specific solution embodies a Black Hole configurations in which light is confined by its intrinsic gravitational pull, distinctively devoid of singularities.

This particular solution detailing Black Holes, contingent upon temporal and radial parameters while featuring discrete spherical energy stratifications, manifests within a radial gravitational field characterized by acceleration directed radially. The intricate interplay among time, radius, and gravitation power is encapsulated within equations (16) and (17), underscoring the nuanced dynamics of Black Holes in this context.

$$\begin{pmatrix} E_r \\ E_\theta \\ E_\varphi \end{pmatrix} = \begin{pmatrix} 0 \\ f(r)\,\mathrm{Sin}(k\,r)\,\mathrm{Sin}(\omega\,t) \\ -f(r)\,\mathrm{Cos}(k\,r)\,\mathrm{Cos}(\omega\,t) \end{pmatrix} \quad \begin{pmatrix} H_r \\ H_\theta \\ H_\varphi \end{pmatrix} = \sqrt{\frac{\varepsilon}{\mu}} \begin{pmatrix} 0 \\ -f(r)\,\mathrm{Sin}(k\,r)\,\mathrm{Cos}(\omega\,t) \\ -f(r)\,\mathrm{Cos}(k\,r)\,\mathrm{Sin}(\omega\,t) \end{pmatrix} \quad \bar{g} = \begin{pmatrix} \frac{G_1}{4\,\pi\,r^2} \\ 0 \\ 0 \end{pmatrix} \tag{16}$$

$$w_{em} = \left(\frac{\mu_0}{2} \left(\bar{m} \cdot \bar{m} \right) + \frac{\varepsilon_0}{2} \left(\bar{e} \cdot \bar{e} \right) \right) =$$

$$f(r)^2 \left(\left(\mathrm{Sin}(k\,r)\,\mathrm{Sin}(\omega\,t) \right)^2 + \left(\mathrm{Cos}(k\,r)\,\mathrm{Cos}(\omega\,t) \right)^2 + \frac{\varepsilon}{\mu} \left(\mathrm{Sin}(k\,r)\,\mathrm{Cos}(\omega\,t) \right)^2 + \left(\mathrm{Cos}(k\,r)\,\mathrm{Sin}(\omega\,t) \right)^2 \right)$$

In which the radial function f(r) equals:

$$f[r] = K\, e^{-\frac{G\, M_{BH}\, \varepsilon_0\, \mu_0}{8\,\pi\,r}} \tag{17}$$

Within the given framework, G represents the Gravitational constant, and M signifies the aggregate electromagnetic mass confined within the Black Hole. Notably, Equation (16) reveals a static electromagnetic field arrangement confined within the system, distinguished by a crucial 90-degree phase discrepancy between the electric

and magnetic fields. This configuration is further illustrated by the presence of distinct Nodes and AntiNodes [13]. The development of this solution has been meticulously carried out in accordance with Newton's Shell Theorem, leading to the genesis of the foundational concept recognized as "Prima Materia" [43].

Assuming a steady speed of light "c" and Planck's constant ħ within the Black Hole, the radius "R" (where n = 1, 2, 3, 4, ...) of the Black Hole possessing the energy equivalent to that of a proton, in accordance with $W = m_{Proton}\, c^2$, is calculated to be $1.5009211 \times 10^{-10}$ [J].

$$R_{GEON} = n\,\lambda = n\left(\frac{c}{f}\right) = n\left(\frac{c}{W}\right)\hbar = 7.1865\ 10^{-26}\left(\frac{n}{W}\right) \tag{18}$$

$$R_{GEON} = n\ 3.82\ 10^{-12}\ [m]$$

Black Holes vary widely in size, ranging from minuscule scales approaching approximately 10^{-27} [kg] as elaborated in detail on Page 39 [33], to immense Black Holes extending to dimensions as large as 10^{40} [kg] as discussed on Page 67 [34]. As Black Holes expand beyond a certain threshold, they transform into what is identified as Dark Matter.

A crucial boundary condition dictating the confinement of Electromagnetic radiation within these Black Hole structures involves achieving a scenario where the energy flux (Poynting vector) reaches a state of equilibrium, reaching zero at the boundary of the confinement. This equilibrium is particularly established at the distinct "90 degrees Phase Shift Surface" in the shape of a sphere. Here, a complex interplay between the Electric Field and the Magnetic Field orchestrates a delicate balance within the confines of the Black Hole

3.1 Black Holes with a Singular point and Large dimensions

Figure 1 depicts a Black Hole with a mass of roughly 10^{35} [kg] and a radius spanning approximately 25 [km]. This particular Black Hole configuration corresponds to a unique mathematical solution derived from equation (8). The radius of this Black Hole is precisely determined to be around 25 [km], a dimension rigorously defined by an alternative mathematical solution outlined within equation (19).

$$f[r] = K\, e^{\left(\frac{G\, M_{BH}\, \varepsilon_0\, \mu_0}{8\, \pi\, r} - \log[r]\right)} \quad [J / m^3] \qquad (19)$$

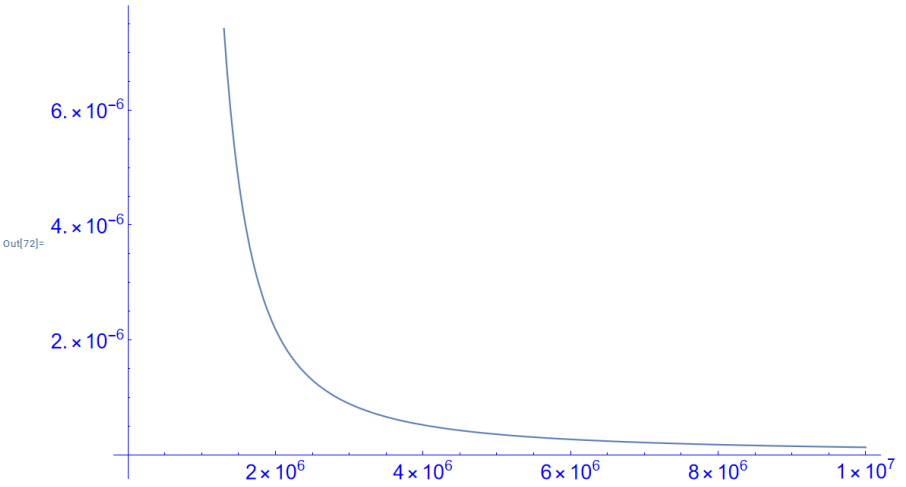

Fig. 1 The Energy Density [J/ m^3] as a function of the Radius R = max 10^7 [m] of the Black Hole.

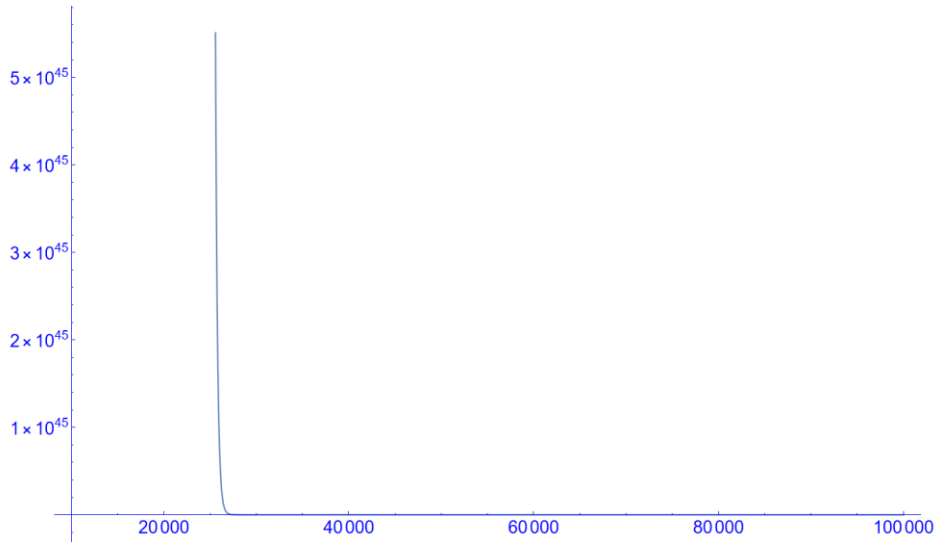

Fig. 2 The Energy Density [J/ m^3] as a function of the Radius R = max 10^5 [m]

Figures 1 and 2 visually portray the significant effects of "Gravitational Intensity Shift" and "Gravitational RedShift" specifically observed at a distance of 25 [km]. Over a vast distance of 10,000 [km], the brightness of light emitted from a Black Hole weighing 10^{35} [kg] gradually diminishes by a factor of 10^{-51}.

Concurrently, the frequency of this emitted light experiences a proportional decline, decreasing by a factor of 10^{-51}. Notably, light initially emitted within the visible spectrum at approximately 10^{14} [Hz] transitions to an exceedingly low frequency of 10^{-37} [Hz]. These extremely low frequencies, associated with remarkably low intensities that have yet to be empirically explored, contribute to the ubiquitous recognition of the term "Black Hole" concerning the phenomena of "Gravitational Intensity Shift" and "Gravitational RedShift" in the presence of substantial masses.

Importantly, it is inferred from equation (8) in conjunction with solutions (10) and (11) that the speed of light remains uniform within and around a Black Hole. The modifications induced by a gravitational field primarily impact the direction of light propagation while preserving the constancy of the speed of light.

3.2 Dark Matter in the Universe controlled by “Gravitational Shielding”

Figure 3 depicts Dark Matter characterized by a collective mass approximately equivalent to 10^{53} [kg] and an expansive radius stretching to roughly ten times the dimensions of the Milky Way Galaxy. The radius of this dark mass is meticulously established to be around 5 x 10^{21} [m], a measure precisely determined by an alternate mathematical solution, denoted as equation (20), derived from equation (8).

$$f[r] = K\ e^{\left(\frac{G\,M_{BH}\ \varepsilon_0\,\mu_0}{8\,\pi\,r}\ -\ \log[r]\right)} \qquad [J / m^3] \tag{20}$$

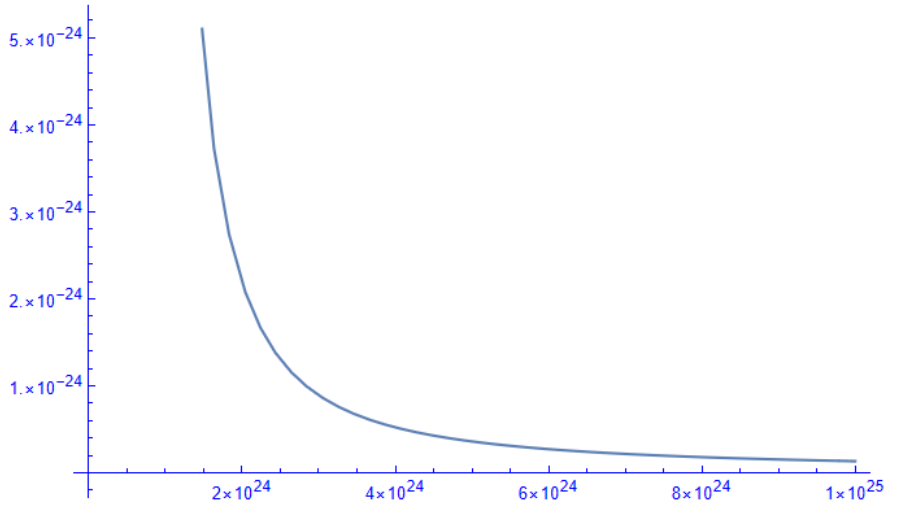

Fig. 3 The Energy Density [J/ m^3] as a function of the Radius R = max 10^{25} [m] of the Dark Matter.

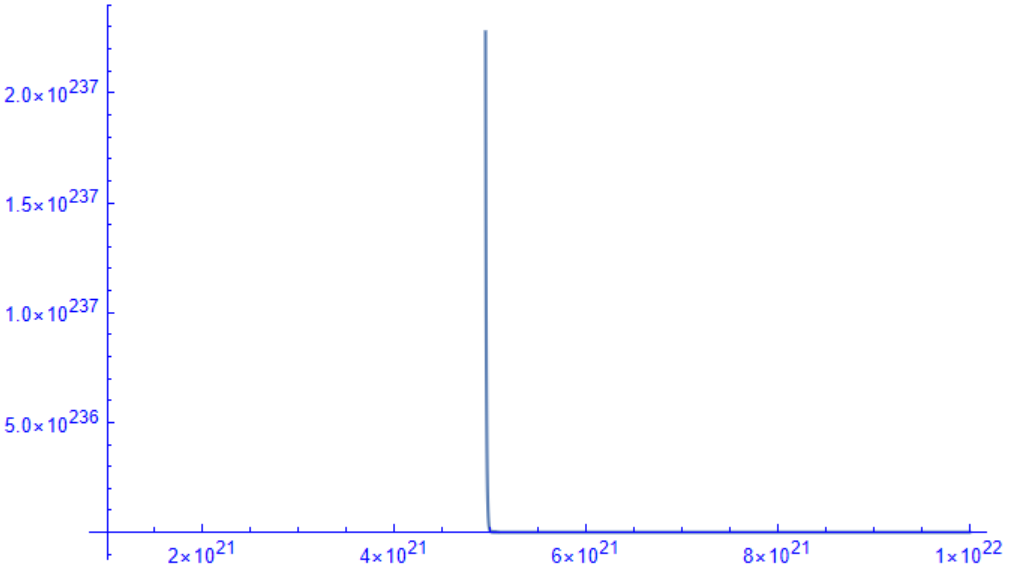

Fig. 4 The Energy Density [J/ m^3] of the Dark Matter as a function of the Radius R = max 10^{22} [m]

Figures 3 and 4 depict the pronounced effects of "Gravitational Intensity Shift" and "Gravitational RedShift" observed at a distance of $5x10^{21}$ [m], which corresponds to 10 times the radius of the Milky Way Galaxy. Across this immense distance, the intensity of light emitted from Dark Matter, featuring a mass of 10^{53} [kg], diminishes significantly by a factor of 10^{-261}.

Similarly, the frequency of the emitted light from the Black Hole experiences an equivalent reduction, declining by a factor of 10^{-261}. Light initially emitted within the visible spectrum at a frequency of 10^{14} [Hz] regresses to an extremely low frequency of 10^{-247} [Hz]. These exceedingly low frequencies, coupled with their incredibly low intensities that remain unmeasured, have prompted the term "Dark Matter" to encapsulate the gravitational effects resulting in "Gravitational Intensity Shift" and "Gravitational RedShift" attributed to immensely massive structures.

It is inferred from equation (8) alongside solutions (10) and (11) that the speed of light remains unchanged within and around the Dark Matter. The gravitational field of the Dark Matter predominantly influences the direction of light propagation while preserving the constancy of the speed of light.

4 The relationship between Black Holes and Quantum Physics

Introducing the Quantum Vector Function $\overline{\phi}$,

$$\overline{\phi} = \sqrt{\frac{\mu}{2}} \left(\overline{H} + i \frac{\overline{E}}{c} \right) \tag{21}$$

Substituting (21) in (16) results in the quantum presentation for the BLACK HOLE:

$$\overline{\Phi(r,\theta,\varphi)} = \sqrt{\frac{\mu}{2}} \left(\overline{H} + i \frac{\overline{E}}{c} \right) f(r) \begin{pmatrix} \Phi_r \\ \Phi_\theta \\ \Phi_\varphi \end{pmatrix} \tag{22}$$

$$\overline{\Phi(r,\theta,\varphi)} = K \sqrt{\frac{\varepsilon}{\mu}} e^{-\frac{G1\, \varepsilon_0\, \mu_0}{8\, \pi\, r}} \begin{pmatrix} 0 & 0 & 0 \\ 0 & -\mathrm{Sin}(k\, r) & \mathrm{Sin}(k\, r) \\ 0 & -i\, \mathrm{Cos}(k\, r) & i\, \mathrm{Cos}(k\, r) \end{pmatrix} \begin{Bmatrix} 0 \\ \mathrm{Cos}\,(\omega\, t) \\ i\, \mathrm{Sin}\,(\omega\, t) \end{Bmatrix}$$

With “K” a constant value dependend of the mass of the BLACK HOLE. The Dot product between the unit vector and the Quantum Vector Function $\overline{\phi}$ represents the quantum mechanical probability function $\Psi[r,t]$ which is a fundamental solution of the Schrödinger Wave Equation.

$$\overline{\Phi(r,\theta,\varphi)} = K \sqrt{\frac{\varepsilon}{\mu}}\, e^{-\frac{G1\,\varepsilon_0\,\mu_0}{8\,\pi\,r}} \begin{pmatrix} 0 & 0 & 0 \\ 0 & -\mathrm{Sin}(k\,r) & \mathrm{Sin}(k\,r) \\ 0 & -i\,\mathrm{Cos}(k\,r) & i\,\mathrm{Cos}(k\,r) \end{pmatrix} \begin{Bmatrix} 0 \\ \mathrm{Cos}\,(\omega\,t) \\ i\,\mathrm{Sin}\,(\omega\,t) \end{Bmatrix} \tag{23}$$

$$\Psi(r,t) = \begin{Bmatrix} 1 & 1 & 1 \end{Bmatrix} \begin{Bmatrix} 0 \\ \mathrm{Cos}\,(\omega\,t) \\ i\,\mathrm{Sin}\,(\omega\,t) \end{Bmatrix} K \sqrt{\frac{\varepsilon}{\mu}}\, e^{-\frac{G1\,\varepsilon_0\,\mu_0}{8\,\pi\,r}} = K \sqrt{\frac{\varepsilon}{\mu}}\, e^{-\frac{G1\,\varepsilon_0\,\mu_0}{8\,\pi\,r}}\, e^{i\,\omega\,t}$$

The Scalar function $\Psi[r,t]$ represents a fundamental solution of the Quantum Mechanical Schrödinger wave equation. [36, 37]

4.1 Black Holes with Discrete Spherical Energy Levels at Sub-Atomic dimensions

In order to effectively confine Electromagnetic Energy, a critical requirement is that the Poynting vector reaches a value of zero at the surface of the spherical confinement. Creating this confinement within a sphere necessitates the presence of a standing electromagnetic wave pattern, characterized by concentric spheres. Each of these spheres establishes an antinodal plane for either the Electric Field (E) or the Magnetic Field (B), with the radius distance between each sphere precisely equal to half the wavelength of the overall confinement.

Within this setup, a constant denoted as "k" is introduced, defined as $k = n\pi\lambda$, where "n" represents a natural number (1, 2, 3, 4, ...) and λ signifies the wavelength of the radiation. This equation elucidates the structured connection between the wavelength, the constant k, and the natural number n within the sphere of electromagnetic confinement in a spherical system.

4.1.1 Time and Radius dependent Black Holes with discrete Energy Levels. The confinements of Electromagnetic Radiation within spherical Regions.

Every concentric sphere represents an anti-nodal surface for the Electric Field (E) or the Magnetic Field (H). The Poynting Vector: $\overline{S} = \overline{E} \times \overline{H}$ at this spherical surface equals zero at any time and at any location at this sphere. The Electromagnetic Energy remains always within this sphere and the next concentric sphere. The concentric spheres have a difference in radius of one half wavelength of the electromagnetic radition within the confinement and a different discrete energy level. Every concentric sphere represents an anti-nodal suface of the electric field or the magnetic field.

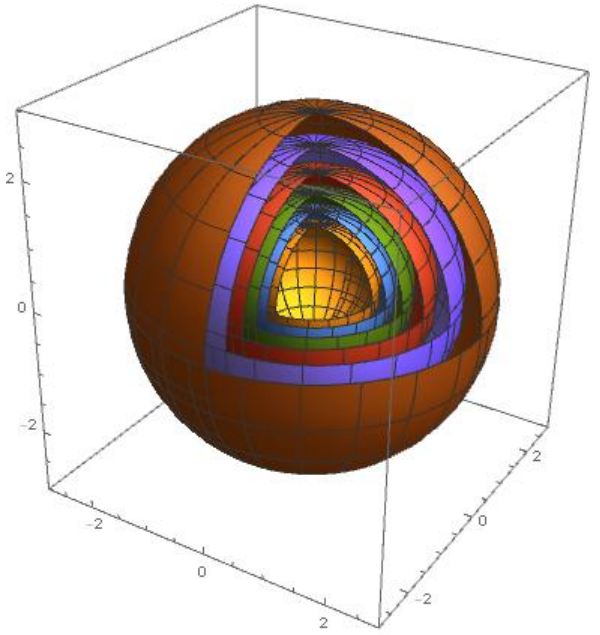

Fig. 5 Nodal and Antinodal Spheres for Standing (Confined) Spherical Electromagnetic waves with a 90 degrees phase shift between the Electric field and the Magnetic field. Equation (23)

Figure 5 illustrates the spatial distribution of nodal and antinodal spheres concerning stationary, confined spherical electromagnetic waves characterized by a distinctive 90-degree phase disparity between the electric and magnetic fields. This configuration is delineated by Equation (23) which encapsulates the nuanced interplay between these fundamental electromagnetic components within a three-dimensional framework.

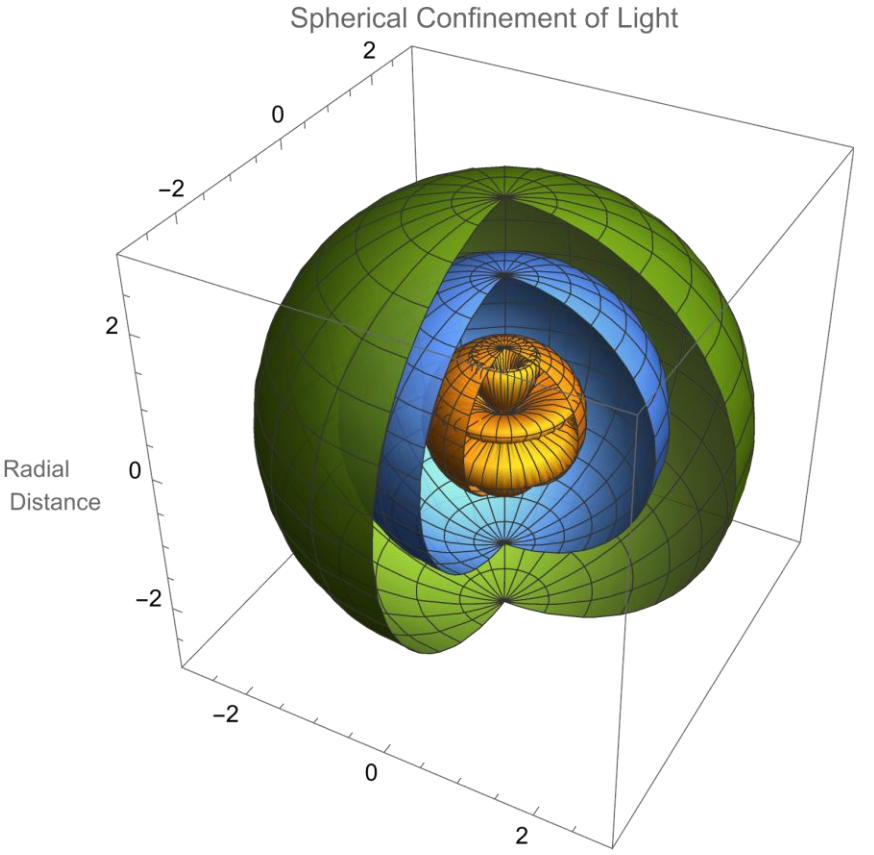

Fig. 6 Nodal- and Anti-nodal Spheres (k = 3) for Standing (Confined) Spherical Electromagnetic waves with a 90 degrees phase shift between the Electric field and the Magnetic field. Equation (23)

Figure 6 depicts the intricate nodal and anti-nodal spheres, emphasizing the scenario of standing, confined spherical electromagnetic waves where the wave number k is set at 3. This visualization captures the unique 90-degree phase offset prevailing between the electric and magnetic fields. Equation (23) serves as the key mathematical representation encapsulating this phenomenon, further elucidating the interplay and characteristics of these electromagnetic waves within a specific spatial context.

Equation (24) describes a Time and Radius dependent BLACK HOLE.

$$\overline{E} = K\, e^{-\frac{G1\varepsilon 0\mu 0}{8\pi r}} \begin{pmatrix} 0 \\ \text{Sin}[k\ r]\ \text{Sin}[\omega\ t] \\ -\text{Cos}[k\ r]\ \text{Cos}[\omega\ t] \end{pmatrix}$$

$$\overline{H} = K\, e^{-\frac{G1\varepsilon 0\mu 0}{8\pi r}} \sqrt{\frac{\varepsilon_0}{\mu_0}} \begin{pmatrix} 0 \\ \text{Sin}[k\ r]\ \text{Cos}[\omega\ t] \\ -\text{Cos}[k\ r]\ \text{Sin}[\omega\ t] \end{pmatrix} \qquad (24)$$

Equation (20) represents by the function $\text{Sin}[k\ r]$ (k = 1,2,3,4….) the confinement of electromagnetic radiation between two concentric spheres. K represents the amplitude of the Electric/ Magnetic Field Intensty. [14]

4.1.2 Time and Polar Angle dependent Black Holes

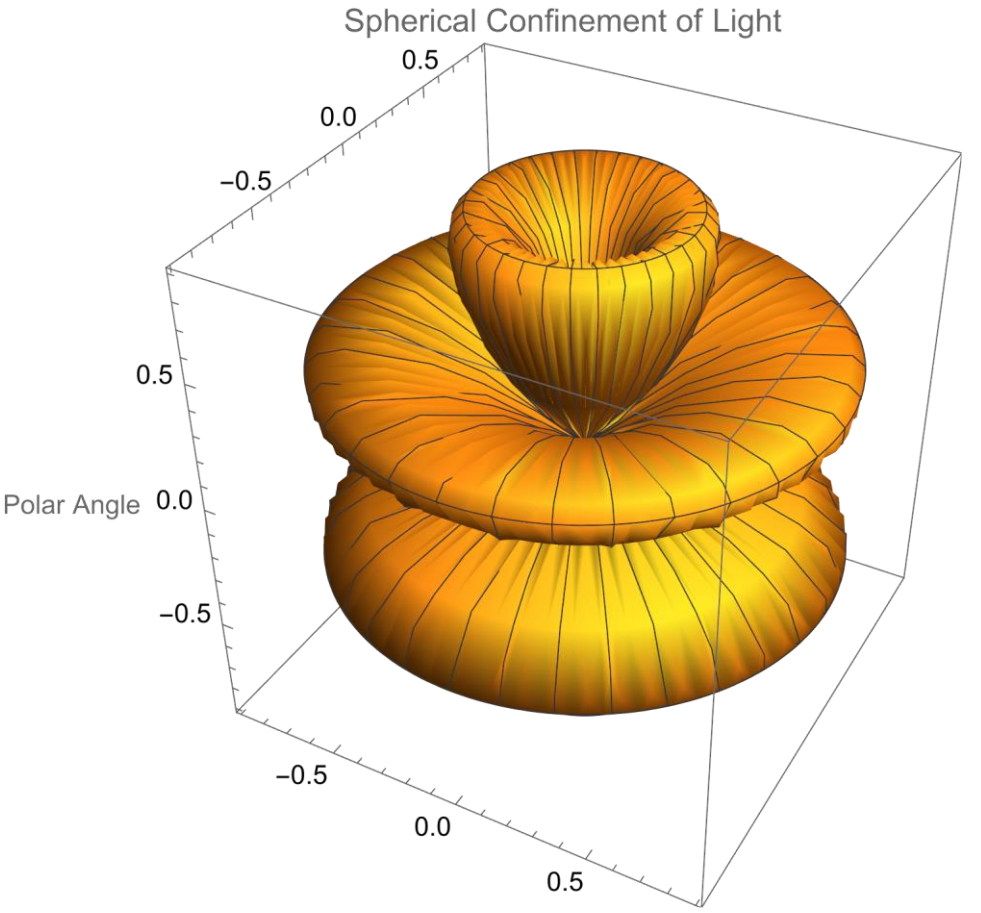

Fig. 7 Nodal- and Antinodal Polar Angle Regions (m = 3) for Standing (Confined) Spherical Electromagnetic waves with a 90 degrees phase shift between the Electric field and the Magnetic field. Equation (15)

In the realm of time and polar angle-dependent black holes, Section 4.1.2 explores the intricate dynamics associated with these celestial entities. Figure 7 offers a detailed insight into the nodal and antinodal regions across the polar angle, particularly emphasizing the case where the azimuthal quantum number m is defined as 3. These findings shed light on the behavior of standing, confined spherical electromagnetic waves featuring a distinct 90-degree phase discrepancy between the electric and magnetic fields, as encapsulated by Equation (25).

Equation (25) describes a Time and “Polar Angle” dependent BLACK HOLE

$$\overline{E} = K\, e^{-\frac{G1\varepsilon 0\mu 0}{8\pi r}} \begin{pmatrix} 0 \\ \text{Sin}[m\ \theta]\ \text{Sin}[\omega\ t] \\ \text{Sin}[m\ \theta]\ \text{Cos}[\omega\ t] \end{pmatrix} \tag{25}$$

$$\overline{H} = K\, e^{-\frac{G1\epsilon 0\mu 0}{8\pi r}} \sqrt{\frac{\varepsilon_0}{\mu_0}} \begin{pmatrix} 0 \\ \text{Sin}[m\ \theta]\ \text{Cos}[\omega\ t] \\ -\text{Sin}[m\ \theta]\ \text{Sin}[\omega\ t] \end{pmatrix}$$

Equation (25) represents by the function $\text{Sin}[m\,\theta]$ (m = 1,2,3,4…..) the confinement of electromagnetic radiation between two Polar Angular Regions [15].

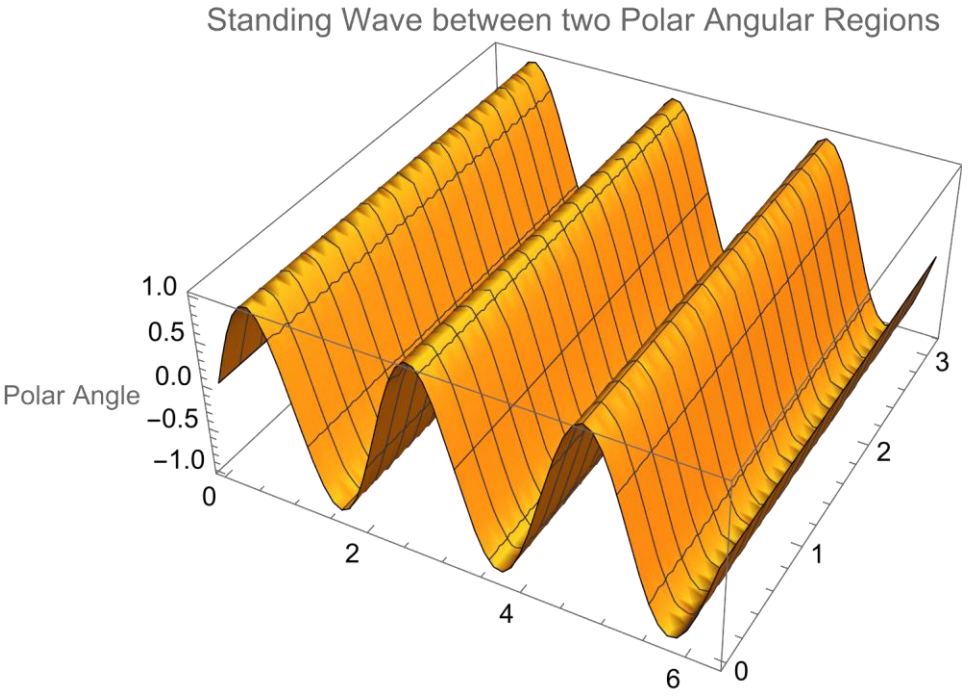

Fig. 8 Nodal- and Antinodal Polar Angle Regions (m = 3) for Standing (Confined) Electromagnetic waves with a 90 degrees phase shift between the Electric field and the Magnetic field. Equation (25)

Figure 8 illustrates the regions of nodal and antinodal behavior with respect to the polar angle, specifically focusing on cases where the azimuthal quantum number m is set to 3. This visualization pertains to standing, confined electromagnetic waves displaying a significant 90-degree phase differential between the electric and magnetic fields. The underlying dynamics are succinctly captured by Equation (15), providing a formal representation of these intriguing wave patterns.

4.1.3 Time and Azimuthal Angular dependent Black Holes

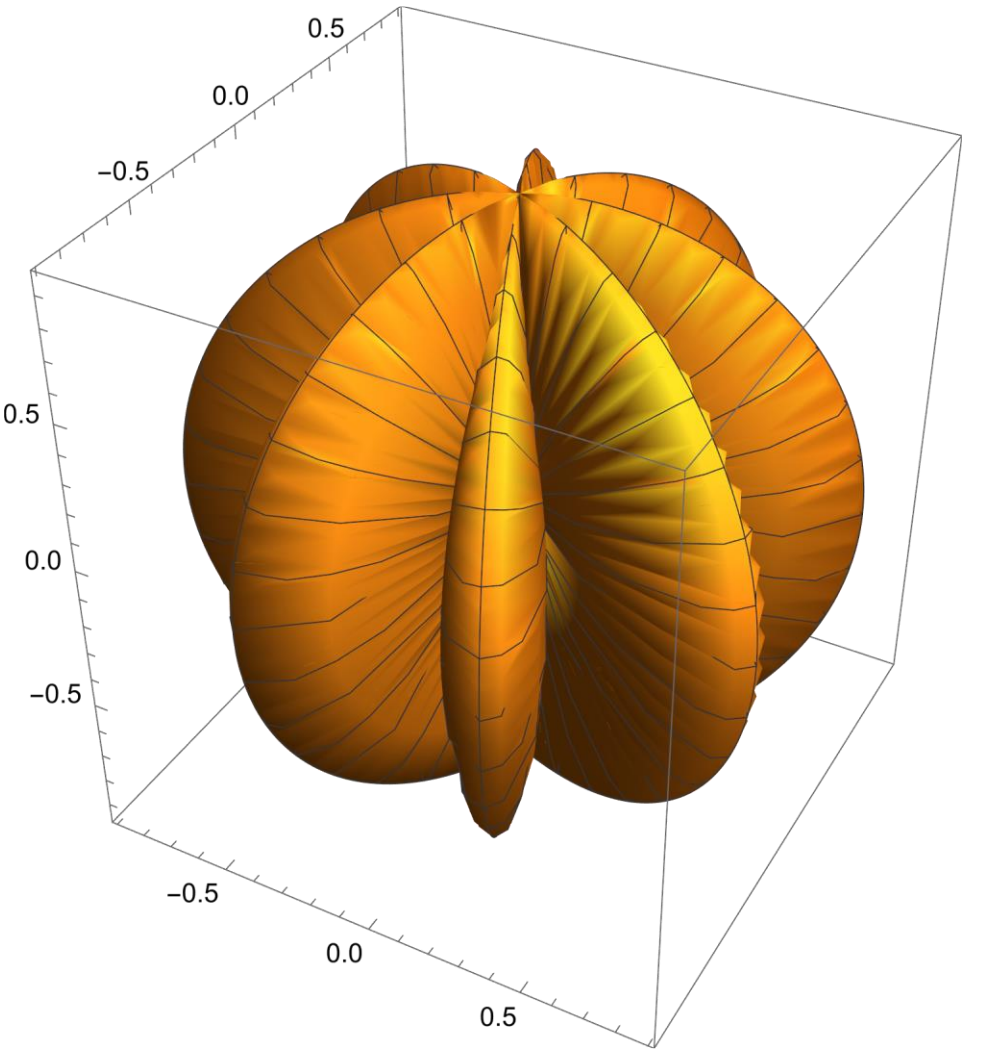

Fig. 9 Nodal- and Antinodal Azimuthal Angular Regions (n = 3) for Standing (Confined) Electromagnetic waves with a 90 degrees phase shift between the Electric field and the Magnetic field. Equation (26)

Fig. 9 Nodal- and Anti-nodal Azimuthal Angular Regions (n = 3) for Standing (Confined) Electromagnetic waves with a 90 degrees phase shift between the Electric field and the Magnetic field. Equation (26).Equation (26) describes a Time and "Polar Angle" dependent BLACK HOLE

$$\overline{E} = K\, e^{-\frac{G1\varepsilon 0\mu 0}{8\pi r}} \begin{pmatrix} 0 \\ \text{Cos}[n\ \varphi]\ \text{Sin}[\omega\ t] \\ \text{Cos}[n\ \varphi]\ \text{Cos}[\omega\ t] \end{pmatrix} \qquad (26)$$

$$\overline{H} = K\, e^{-\frac{G1\epsilon 0\mu 0}{8\pi r}} \sqrt{\frac{\varepsilon_0}{\mu_0}} \begin{pmatrix} 0 \\ \text{Cos}[n\ \varphi]\ \text{Cos}[\omega\ t] \\ -\text{Cos}[n\ \varphi]\ \text{Sin}[\omega\ t] \end{pmatrix}$$

The function denoted by Equation (26), where n ranges over integers (n = 1, 2, 3, ...), encapsulates the confinement of electromagnetic radiation within two distinct Azimuthal Angular Regions, as referenced by [16].

4.1.4 Time, Polar- and Azimuthal Angular dependent Black Holes

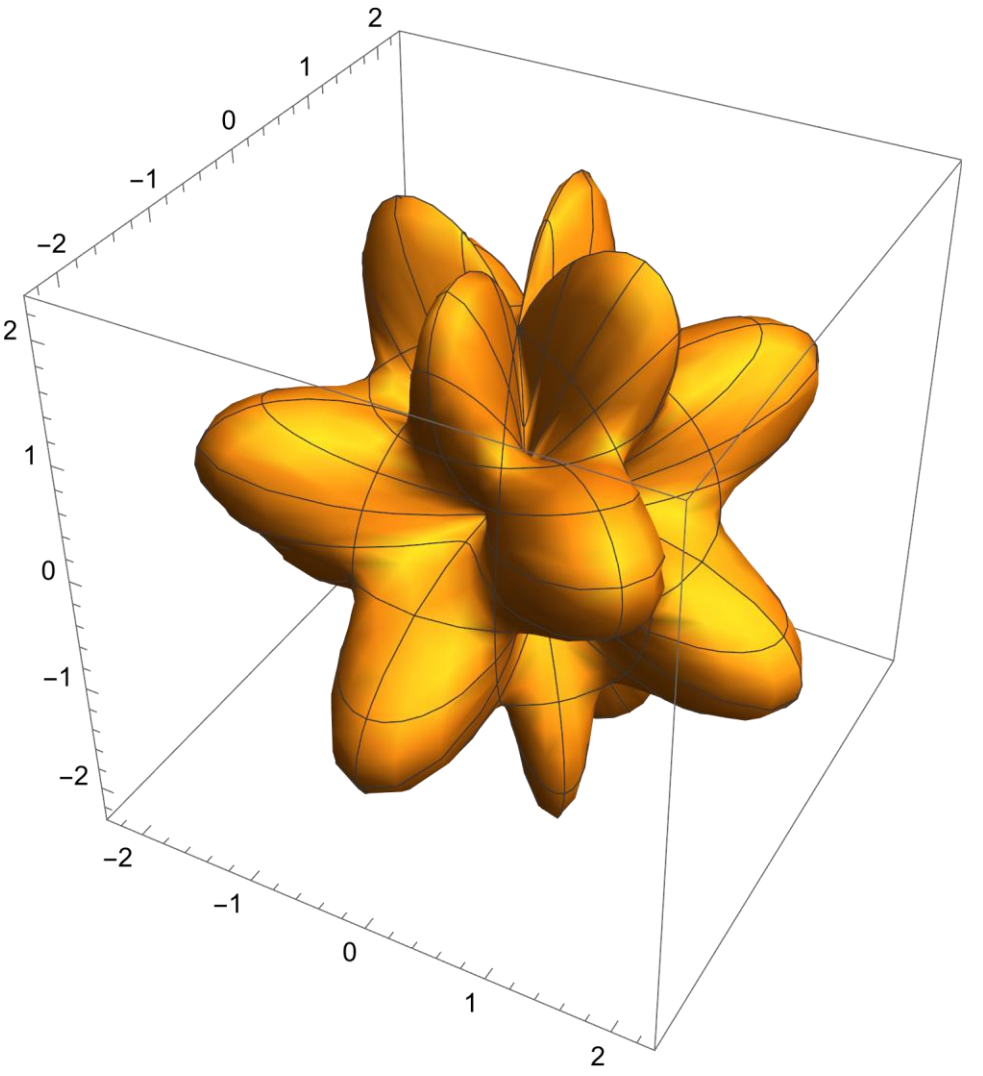

Fig. 10 Nodal- and Anti-nodal Polar Angular and Azimuthal Angular Regions (n = 4 and m = 4) for Standing (Confined) Electromagnetic waves with a 90 degrees phase shift between the Electric field and the Magnetic field. Equation (27)

Figure 10 showcases the delineation of nodal and anti-nodal regions pertaining to both polar and azimuthal angular domains, specifically when n is set to 4 and m is set to 4. This visualization sheds light on the intricate behavior of standing, confined electromagnetic waves characterized by a distinct 90-degree phase difference between the electric and magnetic fields. The mathematical framework governing

these phenomena is encapsulated by Equation (27), providing a formal expression of these electromagnetic wave patterns within the specified angular regions.

Equation (27) describes a Time “Azimuthal Angle” and “Polar Angle” dependent BLACK HOLE

$$\overline{E} = K\, e^{-\frac{G1\varepsilon 0\mu 0}{8\pi r}} \begin{pmatrix} 0 \\ \text{Cos}[n\ \varphi]\ \text{Sin}[m\ \theta]\ \text{Sin}[\omega\ t] \\ \text{Cos}[n\ \varphi]\ \text{Sin}[m\ \theta]\ \text{Cos}[\omega\ t] \end{pmatrix} \tag{27}$$

$$\overline{H} = K\, e^{-\frac{G1\epsilon 0\mu 0}{8\pi r}} \sqrt{\frac{\varepsilon_0}{\mu_0}} \begin{pmatrix} 0 \\ -\text{Cos}[n\ \varphi]\ \text{Sin}[m\ \theta]\ \text{Cos}[\omega\ t] \\ \text{Cos}[n\ \varphi]\ \text{Sin}[m\ \theta]\ \text{Sin}[\omega\ t] \end{pmatrix}$$

Equation (27) represents by the function $\text{Cos}[n\ \varphi]$ (n = 1,2,3,4…..) and $\text{Sin}[m\ \theta]$ (m = 1,2,3,4…..) the confinement of electromagnetic radiation between two Azimuthal Angular Regions and two Polar Angulars Regions [17].

4.1.5 Spherical Confinement of Light beween two Concentric Spheres within Black Holess

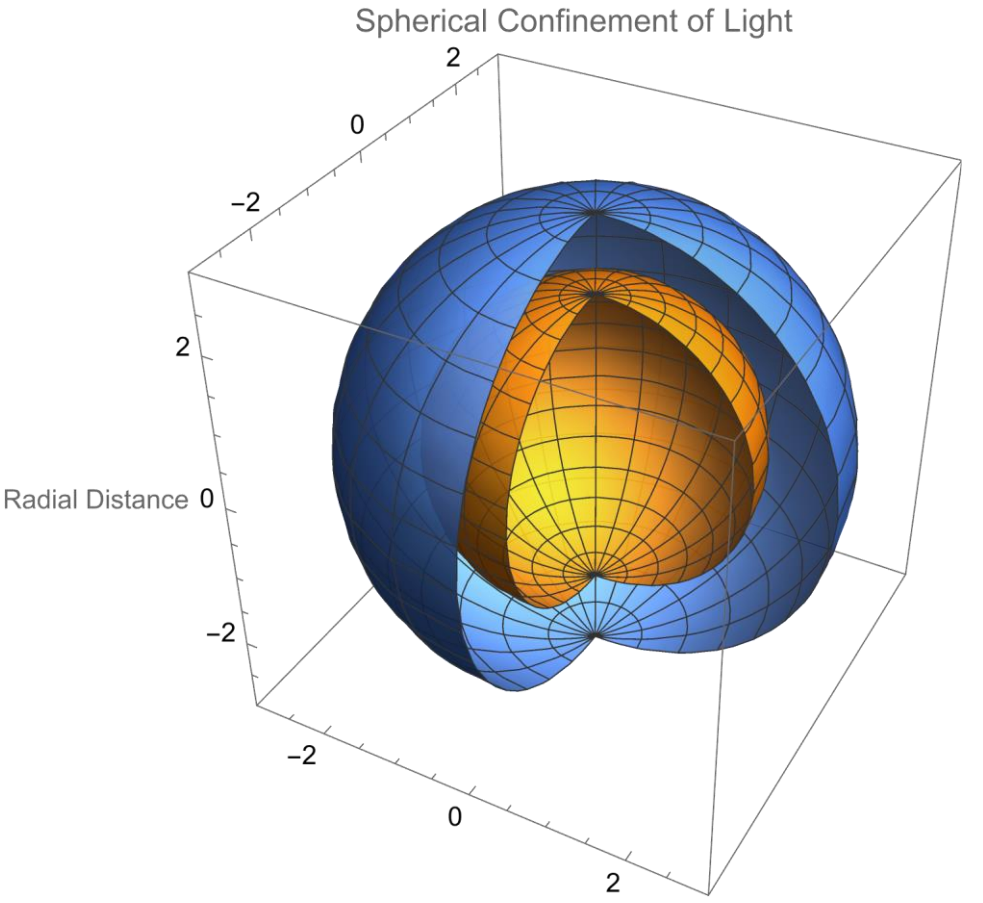

Fig.11 Nodal- and Antinodal Regions for Standing (Confined) Electromagnetic waves with a 90 degrees phase shift between the Electric field and the Magnetic field. Equation (14)

Figure 11 illustrates the nodal and antinodal regions associated with standing, confined electromagnetic waves featuring a 90-degree phase differential between the electric and magnetic fields. The intricacies of this wave behavior are represented mathematically by Equation (14), offering a formal description of the electromagnetic field dynamics within this context.

Equation (28) captures the phenomenon of the reflection of Confined Electromagnetic Energy within the confines of a Black Hole, delineated between two concentric spheres. In this scenario, the speed of light, which is contingent upon the

variable "r" representing the radial distance, undergoes a change in direction commensurate with the frequency of the confined light, or Electromagnetic Radiation.

Remarkably, a Black Hole possesses the capacity to undergo a process of splitting into two distinct Black Holes characterized by differing radii. During this transformation, the original Black Hole transitions to a lower energy level, akin to an atom descending to a lower energy state. The resultant new Black Holes formed as a consequence of this splitting represent the disparity in energy levels, resembling the analogous behavior of an atom transitioning between energy levels within its atomic structure.

$$\bar{E} = K\, e^{-\frac{G1\varepsilon 0\mu 0}{8\pi r}}\, f\left[t - \frac{\sqrt{\varepsilon_0\ \mu_0}\ \text{Cos}[2\ k\ r]}{2\ k}\right] \begin{pmatrix} 0 \\ \text{Sin}[k\ r]\ \text{Sin}[\omega\ t] \\ -\text{Cos}[k\ r]\ \text{Cos}[\omega\ t] \end{pmatrix} \tag{28}$$

$$\bar{H} = K\, e^{-\frac{G1\varepsilon 0\mu 0}{8\pi r}}\, f\left[t - \frac{\sqrt{\varepsilon_0\ \mu_0}\ \text{Cos}[2\ k\ r]}{2\ k}\right] \sqrt{\frac{\varepsilon_0}{\mu_0}} \begin{pmatrix} 0 \\ -\text{Sin}[k\ r]\ \text{Cos}[\omega\ t] \\ -\text{Cos}[k\ r]\ \text{Sin}[\omega\ t] \end{pmatrix}$$

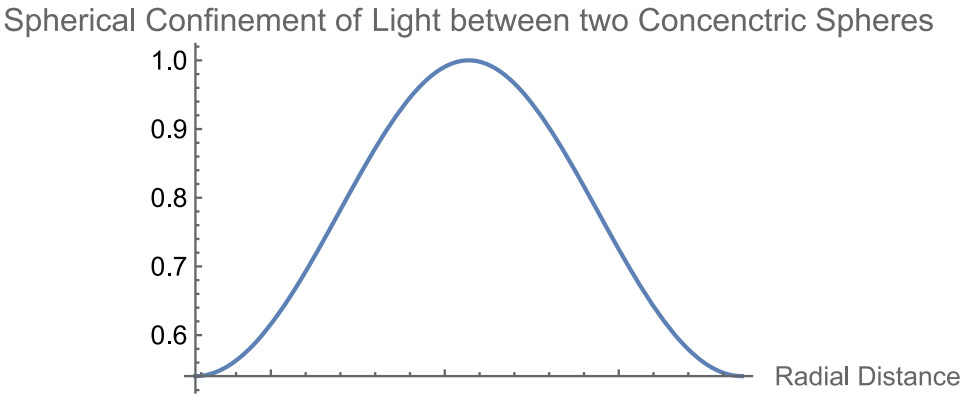

Fig. 12 Nodal- and Antinodal Regions for Standing (Confined) Electromagnetic within two concentric spheres. Equation (18)

Figure 12 presents a visual representation of the nodal and anti-nodal regions characterizing standing, confined electromagnetic waves enclosed within two concentric spheres. The electromagnetic field behaviors within this configuration are mathematically defined by Equation (18), offering a precise formulation of the wave dynamics within the specified spatial constraints.

5 Universal Equilibrium in the "Concept of Quantum Mechanical Probability" in "The New Theory".

The 4-dimensional notation for the divergence of the Stress-Energy Tensor (25) expresses in the 4th dimension (time dimension) the law of Conservation of Energy". For an Electromagnetic Field the law for conservation of Energy has been expressed as:

$$\bar{f}^4 = \begin{pmatrix} f_4 \\ f_3 \\ f_2 \\ f_1 \end{pmatrix} = \square \bullet \bar{\bar{T}} = \begin{pmatrix} \nabla \cdot \bar{S} + \frac{\partial w}{\partial t} \\ f_3 \\ f_2 \\ f_1 \end{pmatrix} = \bar{0}^4 \qquad (29)$$

The derivation of the "Fundamental Equation for Confined Electromagnetic Interaction" in "The New Theory" from the equation governing the Conservation of Electromagnetic Energy (38.1) leads to an expression that mirrors the Relativistic Quantum Mechanical "Dirac" equation as well as the Schrödinger wave equation in scenarios where velocities are considerably lower in comparison to the speed of light.

In the context of "The Proposed Theory," the "Fundamental Equation for Confined Electromagnetic Interaction" can be viewed as the relativistic counterpart of the Quantum Mechanical Schrödinger wave equation, thereby aligning with the Quantum Mechanical Dirac Equation.

5.1 Confined Electromagnetic Energy within a 4-dimensional Equilibrium

The concept of quantum mechanical probability waves was instigated during the notable 1927 5th Solvay Conference. During this era, a convergence of circumstances occurred, culminating in the inception of a distinctive notion of "Material Waves" (solutions of Schrödinger's wave equation) that exhibit complexity, being partially real and partially imaginary. These waves portray the likelihood of the manifestation of a physical entity (such as an elementary particle) and are commonly referred to as "Quantum Mechanical Probability Waves."

The notion of intricate (probability) waves is intimately linked to the idea of confined (standing) waves. An inherent characteristic of any standing acoustical wave is the consistent 90-degree phase shift observed between Velocity and Pressure (analogous to Electric Field and Magnetic Field in Quantum Field Theory). This same principle is mirrored in the context of standing (confined) electromagnetic waves as well.

For that reason every confined (standing) Electromagnetic wave can be described by a complex sum vector $\bar{\phi}$ of the Electric Field Vector $\bar{E}$ and the Magnetic Field Vector $\overline{\mathbf{B}}$ ($\bar{E}$ has 90 degrees phase shift compared to $\overline{\mathbf{B}}$).

The vector functions $\bar{\phi}$ and the complex conjugated vector function $\bar{\phi}^*$ will be written as:

$$\bar{\phi} = \frac{1}{\sqrt{2\,\mu}} \left(\bar{B} + i \frac{\overline{E}}{c} \right) \tag{30}$$

$\overline{\mathbf{B}}$ equals the magnetic induction, $\overline{\mathbf{E}}$ the electric field intensity ($\bar{E}$ has + 90 degrees phase shift compared to $\overline{\mathbf{B}}$) and c the speed of light.

The complex conjugated vector function $\overline{\phi^*}$ equals:

$$\overline{\phi^*} = \frac{1}{\sqrt{2\,\mu}} \left(\bar{B} - i \frac{\overline{E}}{c} \right) \tag{31}$$

The dot product equals the electromagnetic energy density w:

$$\bar{\phi} \cdot \bar{\phi^*} = \frac{1}{2\mu}\left(\bar{B} + i\frac{\bar{E}}{c}\right) \cdot \left(\bar{B} - i\frac{\bar{E}}{c}\right) = \frac{1}{2}\mu H^2 + \frac{1}{2}\varepsilon E^2 = w \qquad (32)$$

Using Einstein's equation $W = m c^2$, the dot product equals the electromagnetic mass density w:

$$\bar{\phi} \cdot \bar{\phi^*}\frac{1}{c^2} = \frac{\varepsilon}{2}\left(\bar{B} + i\frac{\bar{E}}{c}\right)\cdot\left(\bar{B} - i\frac{\bar{E}}{c}\right) = \frac{1}{2}\varepsilon\mu^2 H^2 + \frac{1}{2}\varepsilon^2 E^2 = \rho\ [kg/m^3] \qquad (33)$$

The cross product is proportional to the Poynting vector (Ref. 3, page 202, equation 15).

$$\bar{\phi} \times \bar{\phi^*} = \frac{1}{2\mu}\left(\bar{B} + i\frac{\bar{E}}{c}\right) \times \left(\bar{B} - i\frac{\bar{E}}{c}\right) = i\sqrt{\varepsilon\mu}\ \bar{E} \times \bar{H} = i\sqrt{\varepsilon\mu}\ \bar{S} \qquad (34)$$

This article introduces a novel "Gravitational-Electromagnetic Equation" that delineates Electromagnetic Field Configurations serving as mathematical solutions for both the Scalar Quantum Mechanical Schrödinger Wave Equation and more precisely for the tensor representation of the Relativistic Quantum Mechanical Dirac Equation (41).

The 4-dimensional divergence of the aggregate Electromagnetic Stress-Energy tensor encapsulates the 4-dimensional Force-Density vector. Expressed in units of [N/m^3] across the three spatial coordinates, this vector signifies the outcome of Electro-Magnetic-Gravitational interactions.

$$f^{\mu} = \partial_{\nu} T^{\mu\nu} = 0 \qquad (35)$$

In vector notation the 4-dimensional Force-Density vector can be written as:

$$\bar{f}^4 = \begin{pmatrix} f_4 \\ f_3 \\ f_2 \\ f_1 \end{pmatrix} = \square \bullet \bar{\bar{T}} = 0 \qquad (36)$$

The fundamental boundary condition for this alternative approach to gravity is the requirement that the Force 4 vector equals zero in the 4 dimensions, expressing a universal 4-dimensional equilibrium:

The 3 spatial components of the Force-Density vector stemming from Electro-Magnetic-Gravitational interactions can be expressed as follows:

Upon substituting the electromagnetic values for the electric field intensity "E" and the magnetic field intensity "H" into equation (36), the 4-dimensional representation of the Electro-Magnetic-Gravitational Fields Equation (37) is derived.

Energy-Time Domain

$$\left(f_4\right) \quad \Leftrightarrow \quad \nabla \cdot \left(\bar{E} \times \bar{H}\right) + \frac{1}{2} \frac{\partial\left(\varepsilon_0 \left(\bar{E} \cdot \bar{E}\right) + \mu_0 \left(\bar{H} \cdot \bar{H}\right)\right)}{\partial t} = 0$$

3-Dimensional Space Domain

$$\begin{pmatrix} f_3 \\ f_2 \\ f_1 \end{pmatrix} \quad \Leftrightarrow \quad -\frac{1}{c^2}\frac{\partial\left(\bar{E} \times \bar{H}\right)}{\partial t} + \varepsilon_0 \bar{E}\left(\nabla \cdot \bar{E}\right) - \varepsilon_0 \bar{E} \times \left(\nabla \times \bar{E}\right) + \mu_0 \bar{H}\left(\nabla \cdot \bar{H}\right) - \mu_0 \bar{H} \times \left(\nabla \times \bar{H}\right) = \bar{0} \tag{37}$$

In which f_1 , f_2 , f_3, represent the force densities in the 3 spatial dimensions and f_4 represent the force density (energy flow) in the time dimension (4th dimension). Equation (37) can be written as:

Energy-Time Domain

Conservation of Energy

B-7

$$\left(f_4\right) \qquad \nabla \cdot \bar{S} + \frac{\partial w}{\partial t} = 0 \tag{38.1}$$

3-Dimensional Space Domain

(38)

B-1 B-2 B-3

$$\begin{pmatrix} f_3 \\ f_2 \\ f_1 \end{pmatrix} \quad -\frac{1}{c^2}\frac{\partial\left(\bar{E} \times \bar{H}\right)}{\partial t} + \varepsilon_0 \bar{E}\left(\nabla \cdot \bar{E}\right) - \varepsilon_0 \bar{E} \times \left(\nabla \times \bar{E}\right) +$$

B-4 B-5

$$+\mu_0 \bar{H}\left(\nabla \cdot \bar{H}\right) - \mu_0 \bar{H} \times \left(\nabla \times \bar{H}\right) = \bar{0} \tag{38.2}$$

The 4th term in equation (38.1) can be written in the terms of the Poynting vector "S" and the energy density "w" representing the electromagnetic law for the conservation of energy (Newton's second law of motion).

5.3 The 4-dimensional Relativistic Dirac Equation

Substituting (32) and (34) in Equation (38.1) results in The 4-Dimensional Tensor presentation for the relativistic quantum mechanical Dirac Equation (39):

$$(x_4) \qquad \nabla \cdot (\bar{\phi} \times \bar{\phi}^*) + \frac{i}{c} \frac{\partial \bar{\phi} \cdot \bar{\phi}^*}{\partial t} = 0$$

$$\begin{pmatrix} x_3 \\ x_2 \\ x_1 \end{pmatrix} \quad \frac{i}{c} \frac{\partial (\bar{\phi} \times \bar{\phi}^*)}{\partial t} - \left(\bar{\phi} \times (\nabla \times \bar{\phi}^*) + \bar{\phi}^* \times (\nabla \times \bar{\phi}) \right) + \left(\bar{\phi} (\nabla \cdot \bar{\phi}^*) + \bar{\phi}^* (\nabla \cdot \bar{\phi}) \right) = 0 \qquad (39)$$

To transform the electromagnetic vector wave function $\bar{\phi}$ into a scalar (spinor or one-dimensional matrix representation), the Pauli spin matrices σ and the following matrices (Ref. 3 page 213, equation 99) are introduced:

$$\bar{\alpha} = \begin{bmatrix} 0 & \sigma \\ \sigma & 0 \end{bmatrix} \quad \text{and} \quad \bar{\beta} = \begin{bmatrix} \delta_{ab} & 0 \\ 0 & -\delta_{ab} \end{bmatrix} \qquad (40)$$

The Equations (6), (32) and (34) can be written in tensor presentation as the 4-Dimensional Relativistic Quantum Mechanical Dirac Equation: [3] (Equation 102, page 213)

$$(x_4) \qquad \left(\frac{i m c}{h} \bar{\beta} + \bar{\alpha} \cdot \nabla \right) \psi = -\frac{1}{c} \frac{\partial \psi}{\partial t} \qquad (41.1)$$

$$\begin{pmatrix} x_3 \\ x_2 \\ x_1 \end{pmatrix} \quad -\frac{1}{c^2} \frac{\partial (\bar{E} \times \bar{H})}{\partial t} + \varepsilon_0 \bar{E} (\nabla \cdot \bar{E}) - \varepsilon_0 \bar{E} \times (\nabla \times \bar{E}) + \qquad (41) \qquad (41.2)$$

$$+ \mu_0 \bar{H} (\nabla \cdot \bar{H}) - \mu_0 \bar{H} \times (\nabla \times \bar{H}) + \gamma_0 \bar{g} (\nabla \cdot \bar{g}) - \gamma_0 \bar{g} \times (\nabla \times \bar{g}) = \bar{0}$$

6 The Fundamental Nuclear Plasma-Fusion Stability Equation

Within the realm of thermonuclear-heated plasma, intricate "mechanical-electromagnetic-gravitational interactions" take place between the ionized nuclear plasma, which generates electromagnetic fields within the plasma, and the powerful external field of heating microwave radiation. A critical boundary condition governing the plasma states that, in all directions and at any given moment, the total force densities (measured in N/m^3) must reliably balance out to zero throughout the entire volume encapsulated by the Tokamak structure.

This equilibrium principle highlights the delicate balance required to maintain stability and control within the plasma environment of the Tokamak. By ensuring that the total force densities sum to zero across the plasma volume, researchers and scientists can work towards achieving optimal conditions for efficient nuclear fusion reactions. This fundamental boundary condition plays a pivotal role in understanding and harnessing the forces at play within the plasma to advance fusion energy research towards sustainable and practical applications.

$$\bar{f} = \rho\left(\frac{\partial \bar{v}}{\partial t} + \bar{v}\cdot\nabla\bar{v}\right) + \nabla p - \nabla\cdot\left(\zeta\left(\nabla\bar{v} + (\nabla\bar{v})^{T}\right) - \frac{2}{3}\zeta\,(\nabla\cdot\bar{v})\,\bar{\bar{I}}\right)$$

$$-\varepsilon_0\,\overline{E_E}\,(\nabla\cdot\overline{E_P}) + \mu_0\,\overline{H_E}\times(\nabla\times\overline{H_P}) + \frac{1}{c^2}\frac{\partial\,(\overline{E_E}\times\overline{H_E})}{\partial t} + \frac{1}{c^2}\frac{\partial\,(\overline{E_P}\times\overline{H_P})}{\partial t} + \varepsilon_0\,\overline{E_E}\times(\nabla\times\overline{E_P})$$

$$-\mu_0\,\overline{H_E}\,(\nabla\cdot\overline{H_P}) - \bar{g}\left(\frac{1}{2c^2}\left(\varepsilon E_E^{\,2} + \mu H_E^{\,2}\right)\right) - \gamma_0\,\bar{g}\,(\nabla\cdot\bar{g}) + \gamma_0\,\bar{g}\times(\nabla\times\bar{g}) = \bar{0}\ [\mathrm{N/m^3}]$$

in which:

$\varepsilon_0\,(\nabla\cdot\bar{E}) = \rho_E$ Electric Charge Density $[\mathrm{C/m^3}]$

$\mu_0\,(\nabla\cdot\bar{H}) = \rho_M$ Magnetic Flux Density $[\mathrm{Vs/m^3}]$ or $[\mathrm{Wb/m^3}]$

$\gamma_0\,(\nabla\cdot\bar{g}) = \rho_{Mass}$ Mass Density $[\mathrm{kg/m^3}]$

Electric Energy Density: $w_E = \frac{1}{2}\varepsilon_0 E^2$

Magnetic Energy Density: $w_M = \frac{1}{2}\mu_0 H^2$

Gravitational Energy Density: $w_G = \frac{1}{2}\gamma_0 g^2$

$\bar{g} \triangleq$ acceleration (gravitational, linear- or orbital acceleration)

(42)

In Equation (42), the terms represented in black originate from the foundational Navier-Stokes Equation and Classical Electrodynamics. In contrast, the terms highlighted in red stem from the innovative New Theory, which articulates the intricate "Electro-Magnetic-Accelerated Field" interactions occurring between

matter, such as nuclear plasma, and energy manifested in the electric and magnetic fields.

This breakdown underscores the integration of established principles with groundbreaking theoretical frameworks to comprehensively describe the dynamic interplay between matter and energy within the context of nuclear fusion plasma. By combining these established and novel elements, researchers can delve deeper into understanding the complex mechanisms governing plasma behaviour and strive towards significant advancements in fusion energy research and technology.

In equation (42) represents: $\overline{E_E}$ the external electric field intensity from the induced microwave radiation and the external induced Electric Fields in the DTT configuration with the three superconducting systems: the Toroidal (TF), the Poloidal (PF) Field and Central Solenoid (CS) Field, $\overline{E_P}$ the internal poloidal electric field intensity generated by the charged particles inside the plasma , $\overline{H_E}$ the external magnetic field intensity from the microwave radiation and the externally induced Magnetic Fields in the DTT configuration with the three superconducting systems: the Toroidal (TF), the Poloidal (PF) Field and Central Solenoid (CS) Field , $\overline{H_P}$ the internal (poloidal) magnetic field intensity generated inside the plasma by the spin of the ions, ζ represents the plasma dynamic viscosity, $\overline{v}$ the velocity, $\overline{g}$ the gravitational-, linear- or orbital- acceleration of the electric- and magnetic fields, p the pressure and $\overline{\overline{I}}$ the identity tensor in the Toroidal Tokamak Reactor.

7 Laminar- and Turbulent Plasma Flows

According Maxwell's equation, the magnetic part in Equation (42) can be reduced, only in "Laminar Plasma Flows" into:

$$\mu_0 \overline{H_E} \times (\nabla \times \overline{H_P}) = \mu_0 \overline{H_E} \times \overline{j_P} = \rho \overline{B_E} \times \overline{v} = -\rho \overline{v} \times \overline{B_E} = -\frac{1}{V_{Volume}} q \left(\overline{v} \times \overline{B_E}\right) \quad (43)$$

In which $\overline{j_P}$ the electric current density of the laminar flow of electrically charged particle and "q" the electric charge of the particles.

According Gauss's law, the electric part in Equation (42) can be reduced, only in "Laminar Plasma Flows" into:

$$- \varepsilon_0 \overline{E_E} (\nabla . \overline{E_P}) = - \overline{E_E} (\nabla . \overline{D_P}) = - \overline{E_E} \rho = - \frac{1}{V_{Volume}} q_P \overline{E_E} \qquad (44)$$

Substituting (43) and (44) in (42) (only valid in laminar Plasma Flows) results in :

$$\bar{f} = \rho \left(\frac{\partial \bar{v}}{\partial t} + \bar{v} \cdot \nabla \bar{v} \right) + \nabla p - \nabla \cdot \left(\zeta \left(\nabla \bar{v} + (\nabla \bar{v})^T \right) - \frac{2}{3} \zeta (\nabla \cdot \bar{v}) \bar{\bar{I}} \right)$$

$$- \frac{1}{V_{Volume}} q_P \left(\overline{E_E} + \bar{v} \times \overline{B_E} \right) + \frac{1}{c^2} \frac{\partial (\overline{E_E} \times \overline{H_E})}{\partial t} + \frac{1}{c^2} \frac{\partial (\overline{E_P} \times \overline{H_P})}{\partial t} + \varepsilon_0 \overline{E_E} \times (\nabla \times \overline{E_P})$$

$$- \mu_0 \overline{H_E} (\nabla . \overline{H_P}) - \bar{g} \left(\frac{1}{2 c^2} \left(\varepsilon E_E^2 + \mu H_E^2 \right) \right) - \gamma_0 \bar{g} (\nabla . \bar{g}) + \gamma_0 \bar{g} \times (\nabla \times \bar{g}) = \bar{0} \; [N/m^3]$$

in which:

$\varepsilon_0 (\nabla . \bar{E}) = \rho_E$ Electric Charge Density $[C/m^3]$

$\mu_0 (\nabla . \bar{H}) = \rho_M$ Magnetic Flux Density $[Vs/m^3]$ or $[Wb/m^3]$

$\gamma_0 (\nabla . \bar{g}) = \rho_{Mass}$ Mass Density $[kg/m^3]$

Electric Energy Density: $w_E = \frac{1}{2} \varepsilon_0 E^2$

Magnetic Energy Density: $w_M = \frac{1}{2} \mu_0 H^2$

Gravitational Energy Density: $w_G = \frac{1}{2} \gamma_0 g^2$

$\bar{g} \triangleq$ acceleration (gravitational, linear- or orbital acceleration)

(45)

In equation (45), the black-colored terms are derived from the Navier-Stokes Equation and Classical Electrodynamics. The red-colored terms, however, arise from the New Theory, which describes "Electro-Magnetic-Accelerated Field" interactions between matter (nuclear plasma) and energy (electric and magnetic fields).

In the context of turbulent plasma flows, only Equation (42) is applicable.

8 Rotations of the Nuclear Plasma

A characteristic effect of the Nuclear Plasma, confined in a “Tokamak Reactor”, are the rotations of the Confined Nuclear Plasma in the Polar Direction and the Angular direction in Toroidal Coordinates [r, θ ,ϕ, α] . In which [θ] represents the angle in the polar direction and [ϕ] represents the angle of rotation in the azimuthal direction. The local radius has been represented by [r] and the radius of the Torus by [α] .

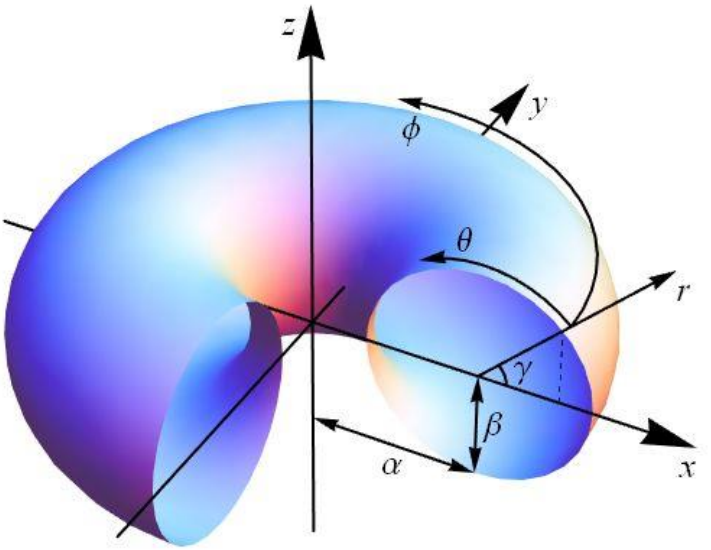

$$(r, \theta, \phi) = \left(\sqrt{\left(\sqrt{x^2 + y^2} - \alpha \right)^2 + z^2} \, , \left(\tan^{-1} \frac{z}{\sqrt{x^2 + y^2} - \alpha} \right) - \gamma, \tan^{-1} \frac{y}{x} \right)$$

$$(x, y, z) = ((\alpha + r \cos(\theta + \gamma)) \cos \phi, (\alpha + r \cos(\theta + \gamma)) \sin \phi, r \sin(\theta + \gamma))$$

Fig. 13 Representation of Toroidal Coordinates

The force density, expressed in [N/ m^3], causing the rotation of the Plasma in the Polar direction follows from equation (42) and has been represented in the color red and the force density, expressed in [N/ m^3], causing rotation of the Plasma in the Azimuthal direction has been represented in the color green.

$$\bar{f} = \rho\left(\frac{\partial \bar{v}}{\partial t} + \bar{v}\cdot\nabla\bar{v}\right) + \nabla p - \nabla\cdot\left(\zeta\left(\nabla\bar{v} + (\nabla\bar{v})^T\right) - \frac{2}{3}\zeta(\nabla\cdot\bar{v})\bar{\bar{I}}\right)$$
$$- \varepsilon_0 \overline{E_E}(\nabla\cdot\overline{E_P}) + \mu_0 \overline{H_E}\times(\nabla\times\overline{H_P}) + \frac{1}{c^2}\frac{\partial(\overline{E_E}\times\overline{H_E})}{\partial t} + \frac{1}{c^2}\frac{\partial(\overline{E_P}\times\overline{H_P})}{\partial t} + \varepsilon_0\overline{E_E}\times(\nabla\times\overline{E_P})$$
$$- \mu_0\overline{H_E}(\nabla\cdot\overline{H_P}) - \bar{g}\left(\frac{1}{2c^2}\left(\varepsilon E_E^2 + \mu H_E^2\right)\right) - \gamma_0\bar{g}(\nabla\cdot\bar{g}) + \gamma_0\bar{g}\times(\nabla\times\bar{g}) = \bar{0}\ [N/m^3] \qquad [46]$$

in which:

$\varepsilon_0(\nabla\cdot\bar{E}) = \rho_E$ Electric Charge Density [C/ m^3]

$\mu_0(\nabla\cdot\bar{H}) = \rho_M$ Magnetic Flux Density [Vs/ m^3] or [Wb/ m^3]

$\gamma_0(\nabla\cdot\bar{g}) = \rho_{Mass}$ Mass Density [kg/ m^3]

Electric Energy Density: $w_E = \frac{1}{2}\varepsilon_0 E^2$

Magnetic Energy Density: $w_M = \frac{1}{2}\mu_0 H^2$

Gravitational Energy Density: $w_G = \frac{1}{2}\gamma_0 g^2$

$\bar{g} \triangleq$ acceleration (gravitational, linear- or orbital acceleration)

The force density, expressed in [N/ m^3] causing the rotation of the Plasma in the Polar direction has been expressed by Equation [47]:

$$\overline{f_{Polar\ Rotation}} = -\varepsilon_0\overline{E_{External}}(\nabla\cdot\overline{E_P}) + \mu_0\overline{H_{Tokamak}}\times(\nabla\times\overline{H_P})\ [N/m^3] \qquad [47]$$

In which the predominant terms, caused by the strong magnetic field inside the Tokamak, are colored magenta.

The force density, expressed in [N/ m^3] causing the rotation of the Plasma in the Azimuthal Direction has been expressed by Equation [48]:

$$\overline{f_{Azimuthal\ Rotation}} = -\mu_0\overline{H_{Tokamak}}(\nabla\cdot\overline{H_P}) + \varepsilon_0\overline{E_{External}}\times(\nabla\times\overline{E_P})\ [N/m^3] \qquad [48]$$

9 Equilibrium within Electromagnetically Confined Nuclear Plasma

From Equation (38) follows the 4-dimensional Electromagnetic-Dynamical Equilibrium Equation for Electromagnetically Confined Nuclear Plasma:

Energy-Time Domain

$$\nabla \cdot \bar{S} + \frac{\partial w}{\partial t} = 0 \qquad [N/m^2\,s]$$

3-Dimensional Space Domain

$$\begin{aligned} \bar{f} &= \rho\left(\frac{\partial \bar{v}}{\partial t} + \bar{v}\cdot\nabla\bar{v}\right) + \nabla p - \nabla\cdot\left(\zeta\left(\nabla\bar{v} + \left(\nabla\bar{v}\right)^T\right) - \frac{2}{3}\zeta\left(\nabla\cdot\bar{v}\right)\bar{\bar{I}}\right) \\ &- \varepsilon_0\,\overline{E_E}\,(\nabla\cdot\overline{E_P}) + \mu_0\,\overline{H_E}\times(\nabla\times\overline{H_P}) + \frac{1}{c^2}\frac{\partial\,(\overline{E_E}\times\overline{H_E})}{\partial t} + \frac{1}{c^2}\frac{\partial\,(\overline{E_P}\times\overline{H_P})}{\partial t} + \varepsilon_0\,\overline{E_E}\times(\nabla\times\overline{E_P}) \\ &- \mu_0\,\overline{H_E}\,(\nabla\cdot\overline{H_P}) - \bar{g}\left(\frac{1}{2c^2}\left(\varepsilon E_E^{\,2} + \mu H_E^{\,2}\right)\right) - \gamma_0\,\bar{g}\,(\nabla\cdot\bar{g}) + \gamma_0\,\bar{g}\times(\nabla\times\bar{g}) = \bar{0}\ [N/m^3] \end{aligned} \tag{49}$$

Which can be written a:

Energy-Time Domain

$$\nabla\cdot(\overline{E_P}\times\overline{H_P}) + \frac{1}{2}\frac{\partial\left(\varepsilon E_E^{\,2} + \mu H_E^{\,2}\right)}{\partial t} = 0 \qquad [N/m^2\,s]$$

3-Dimensional Space Domain

$$\begin{aligned} \bar{f} &= \rho\left(\frac{\partial \bar{v}}{\partial t} + \bar{v}\cdot\nabla\bar{v}\right) + \nabla p - \nabla\cdot\left(\zeta\left(\nabla\bar{v} + \left(\nabla\bar{v}\right)^T\right) - \frac{2}{3}\zeta\left(\nabla\cdot\bar{v}\right)\bar{\bar{I}}\right) \\ &- \varepsilon_0\,\overline{E_E}\,(\nabla\cdot\overline{E_P}) + \mu_0\,\overline{H_E}\times(\nabla\times\overline{H_P}) + \frac{1}{c^2}\frac{\partial\,(\overline{E_E}\times\overline{H_E})}{\partial t} + \frac{1}{c^2}\frac{\partial\,(\overline{E_P}\times\overline{H_P})}{\partial t} + \varepsilon_0\,\overline{E_E}\times(\nabla\times\overline{E_P}) \\ &- \mu_0\,\overline{H_E}\,(\nabla\cdot\overline{H_P}) - \bar{g}\left(\frac{1}{2c^2}\left(\varepsilon E_E^{\,2} + \mu H_E^{\,2}\right)\right) - \gamma_0\,\bar{g}\,(\nabla\cdot\bar{g}) + \gamma_0\,\bar{g}\times(\nabla\times\bar{g}) = \bar{0}\ [N/m^3] \end{aligned} \tag{50}$$

9. Conclusions

In the realm of nuclear fusion, achieving equilibrium within the plasma environment is vital for understanding the complexities and dynamics of fusion reactions. This equilibrium, crucial for stability, involves a delicate interplay of various forces within the nuclear plasmas.

The fusion of nuclei in a plasma introduces a new perspective on equilibrium, where electromagnetic, gravitational, and mechanical forces interact in intricate ways. Understanding and maintaining this equilibrium are critical for ensuring the success of nuclear fusion processes, especially within advanced confinement systems like Tokamaks.

To navigate the challenges and optimize nuclear fusion, a fresh theoretical approach is imperative. By integrating electromagnetic, gravitational, and mechanical force density interactions into models like the Navier-Stokes equation and Equation 42, researchers can more accurately predict and control the equilibrium within nuclear plasmas.

Furthermore, achieving three-dimensional equilibrium, as outlined in equations 42 and 45, is a fundamental step in stabilizing nuclear fusion reactions. This equilibrium among dynamic and electromagnetic force densities within the plasma forms the basis for ensuring the efficiency and sustainability of fusion energy technologies.

As we delve deeper into the complexities of plasma equilibrium in nuclear fusion, we move closer to unlocking the full potential of fusion energy as a viable and environmentally friendly power source. By continuously refining our understanding of equilibrium within nuclear plasmas, we pave the way for a future powered by safe and abundant fusion energy.

- General Relativity, based on the zero rest mass of photons, explicates the interaction between Gravity and Light within a 4-dimensional spacetime curvature shaped by gravitational fields, guiding the trajectory of light through curved geometries.
-
- The new theory introduces a dual separation between mass and inertia for light (photons): inertia is exclusively present along the beam's propagation axis, determining light speed, while mass is perpendicular to propagation, influencing light deflection by gravitational fields.
-
- Black Holes, serving as gravitational-electromagnetic confinements, are solutions of the relativistic quantum mechanical Dirac equation, demonstrating

the significant effects of Gravitational Intensity Shift and Gravitational RedShift. Detecting these phenomena demands extremely sensitive observatories operating at low frequency ranges.

- The new theory investigates the impact of "CURL" within gravitational fields near Black Holes, affecting Gravitational Lensing in a manner not accounted for by General Relativity.
-
- Operating within a 4-dimensional equilibrium and considering force densities, Black Holes at sub-atomic scales manifest as tangible entities, providing solutions to the Relativistic Quantum Mechanical Dirac Equation with discrete energy levels.
-
- Experimental validation involving the comparison of Gravitational RedShift calculations between General Relativity and the new theory in Earth's gravitational field, though demanding, requires highly precise instrumentation.
-
- Dark Matter's presence is affirmed by the gravitational repercussions of Gravitational RedShift and Gravitational Intensity Shift, rendering galaxies invisible beyond a specific gravitational shielding distance due to mass-influenced effects on light emission.

- Ongoing experiments aimed at verifying the new theory's predictions are in progress, with results pending publication following extensive scrutiny by multiple scientific bodies to discern the implications of observed interference pattern fluctuations. Global collaboration among scientific teams is crucial for the comprehensive assessment of these experimental outcomes.

5.1 Data Availability

All Data and Calculations have been published at:

https://quantumlight.science/

References

[1] Wheeler; John Archibald; GEONs, Physical Review Journals Archive, 97, 511, Issue 2, pages 511-526, Published 15 January 1955, Publisher: American Physical Scociety, DOI: 10.1103/PhysRev.97.511:

[2] Sven Herrmann, Felix Finke, Martin Lülf, Olga Kichakova, Dirk Puetzfeld, Daniela Knickmann, Meike List, Benny Rievers, Gabriele Giorgi, Christoph Günther, Hansjörg Dittus; Test of the Gravitational Redshift with Galileo Satellites in an Eccentric Orbit ;Phys. Rev. Lett. **121**, 231102 – Published 4 December 2018; Gravitational Redshift Test Using Eccentric Galileo Satellites, DOI: 10.1103/PhysRevLett.121.231102

[3] Vegt Wim;. A Continuous Model of Matter based on AEONs, Physics Essays, Volume 8, Number 2, 1995, DOI: 10.31219/osf.io/ra7ng

[4] Vegt Wim; Mathematical Solutions for the Propagation of Light in Quantum Light Theory, Calculations in Mathematica 13.1: https://community.wolfram.com/groups/-/m/t/2576692?p_p_auth=mTldHX3v

[5] Vegt Wim; Gravitational RedShift between two Atomic Clocks, Calculations in Mathematica 13.1: https://community.wolfram.com/groups/-/m/t/2622560?p_p_auth=EC8QO0Xz

[6] Vegt Wim; Propagation of Light within a Gravitational Field in Quantum Light Theory, Calculation in Mathematica 13.1: https://community.wolfram.com/groups/-/m/t/2576537?p_p_auth=iljE3giH

[7] Raymond J. Beach; A Classical Field Theory of Gravity and Electromagnetism; Journal of Modern Physics, Vol.5 No.10, June 2014

[8] Maxwell James Clerk; A dynamical theory of the electromagnetic field; 01 January 1865; https://royalsocietypu blishing.org/doi/10.1098/rstl.1865.0008

[9] A. Einstein; On the Influence of Gravitation on the Propagation of Light; Annalen der Physik (ser. 4), **35**, 898–908, http://myweb.rz.uni-augsburg.de/~eckern/adp/history/einstein-papers/1911_35_898-908.pdf

[10] Mahendra Goray, Ramesh Naidu Annavarapu, Rest mass of photon on the surface of matter, Results in Physics 16 (202) 102866, January 2020, DOI: 10.1016/j.rinp.2019.102866

[11] Antonio Genova, Erwan Mazarico, Sander Goossens, Frank G. Lemoine, Gregory A. Neumann, David E. Smith & Maria T. Zuber; Solar system expansion and strong equivalence principle as seen by the NASA MESSENGER mission; Nat Commun 9; 289 (2018). DOI: 10.1038/s41467-017-02558-1

[12] John G. Williamson; A new linear theory of light and matter; 2019; J. Phys.: Conf. Ser. 1251 012050 DOI 10.1088/1742-6596/1251/1/012050
[13] Vegt Wim; Black Holes with Discrete Spherical Energy Levels: https://community.wolfram.com/groups/-/m/t/2896941?p_p_auth=D7ZKuo3k
[14] Vegt Wim; Time and Radius dependent GEONs with discrete Energy Levels https://community.wolfram.com/groups/-/m/t/2900869?p_p_auth=yxR9nZu6
[15] Vegt Wim; Time and Angular Regions dependent GEONs with discrete energy levels. https://community.wolfram.com/groups/-/m/t/2901457?p_p_auth=H4jjDHmQ
[16] Vegt Wim; Time and Azimuthal Regions dependent GEONs with discrete energy levels https://community.wolfram.com/groups/-/m/t/2902170?p_p_auth=yt0q5nEh
[17] Vegt Wim; Time, Polar Angular and Azimuthal Angular Regions dependent GEONs with discrete energy levels https://community.wolfram.com/groups/-/m/t/2902642?p_p_auth=sW2mvv9L
[18] D. W. Sciama; The Physical Structure of General Relativity; Rev. Mod. Phys. 36, 463 – Published 1 January 1964; Erratum Rev. Mod. Phys. 36, 1103 (1964)
[19] Adrian del Rio, Jose Navarro-Salas, and Francisco Torrenti; Renormalized stress-energy tensor for spin -1/2 fields in expanding universes; Phys. Rev. D 90, 084017 – Published 13 October 2014
[20] Stergios Pellis; Unity Formulas for the Coupling Constants and the Dimensionless Physical Constants; Journal of High Energy Physics Gravitation and Cosmology; DOI: 10.4236/jhepgc.2023.91021
[21] Bloch, Yakov and Joshua Foo. "How the result of a measurement of a photon's mass can turn out to be 100." (2023). Corpus ID: 258426255
[22] Andrés Arámburo García, Kyrylo Bondarenko, Sylvia Ploeckinger, Josef Pradler and Anastasia Sokolenko; Effective photon mass and (dark) photon conversion in the inhomogeneous Universe; Journal of Cosmology and Astroparticle Physics, Volume 2020, October 2020
[23] Alexander M Gabovich and Nadezhda A Gabovich; How to explain the non-zero mass of electromagnetic radiation consisting of zero-mass photons; European Journal of Physics; 2007; 28 649; DOI 10.1088/0143-0807/28/4/004
[24] Liang-Cheng Tu, Jun Luo and George T Gillies; The mass of the photon; Reports on Progress in Physics, Volume 68, Number 1; DOI 10.1088/0034-4885/68/1/R02
[25] Doyon B; Conformal Loop Ensembles and the Stress–Energy Tensor. Lett Math Phys 103, 233–284 (2013). https://doi.org/10.1007/s11005-012-0594-1
[26] T. P. Hack and V. Moretti; On the stress–energy tensor of quantum fields in curved spacetimes—comparison of different regularization schemes and symmetry of the Hadamard/Seeley–DeWitt coefficients; 2012 J. Phys. A: Math. Theor. 45 374019; DOI: 10.1088/1751-8113/45/37/374019
[27] Adam Levi; Renormalized stress-energy tensor for stationary black holes;

Phys. Rev. D 95, 025007 – Published 10 January 2017; https://doi.org/10.1103/PhysRevD.95.025007
[28] Gobbi, Julio; Luminiferous Æther: General Science Journal; December 10, 2018
γ_0 = Gravitational permeability of vacuum [kg s2 m-3]
[29] Xing-Hao Ye, Qiang Lin; Gravitational Lensing Analyzed by Graded Refractive Index of Vacuum; Journal of Optics A: Pure and Applied Optics; 1 May 2008; DOI 10.1088/1464-4258/10/7/075001
[30] Vegt Wim; "The Origin of Gravity in "Quantum Light Theory""; OSF Preprints; October 14. doi:10.31219/osf.io/n43yd
[31] P. Delva, N. Puchades, E. Schönemann, F. Dilssner, C. Courde, S. Bertone, F. Gonzalez, A. Hees, Ch. Le Poncin-Lafitte, F. Meynadier, R. Prieto-Cerdeira (et. all); Gravitational Redshift Test Using Eccentric Galileo Satellites; Phys. Rev. Lett. 121, 231101 – Published 4 December 2018; DOI: 10.1103/PhysRevLett.121.231101
[32] Oppenheim, Jonathan, A Postquantum Theory of Classical Gravity, Phys. Rev. X, Vol. 13, December 2023; DOI: https://doi.org/10.1103/PhysRevX.13.041040
[33] Vegt Wim, The Origin of Gravity, A second order Lorentz Transformation for "Accelerated Electromagnetic Fields", Generating a Gravitational Field and the property of Mass, International Research Journal of Pure and Applied Physics Vol.9 No.1, pp.12-52, 2022.
[34] Vegt Wim, The 4-Dimensional Dirac Equation in Relativistic Field Theory, European Journal of Applied Sciences, Vol 9, No. 1, pp 35 – 93,2021
[35] Vegt Wim; A Perfect Equilibrium inside a Black Hole; Wolfram Community: https://community.wolfram.com/groups/-/m/t/3087823?p_p_auth=dpH7iBMg
[36] Einstein Albert; "Elementare Uberlegungen zur Interpretation der Grundlagen der Quanten-Mechanik", Translated into English, 2011, DOI: https://doi.org/10.48550/arXiv.1107.3701
[37] Nikko John Leo S. Lobos, Reggie C. Pantig; Generalized Extended Uncertainty Principle Black Holes: Shadow and lensing in the macro- and microscopic realms; Physics 2022, 4(4), 1318-1330; https://doi.org/10.3390/physics4040084
[38] Zihua Weng; Influence of velocity curl on conservation laws, October 2008, arXiv:0810.0065. https://doi.org/10.48550/arXiv.0810.0065
[39] Peter Vadasz; Rendering the Navier–Stokes Equations for a Compressible Fluid into the Schrödinger Equation for Quantum Mechanics, MDPI-Fluids, May 2016, https://doi.org/10.3390/fluids1020018
[40] Young-Sam Kwon; Asymptotic limit for rotational quantum compressible Navier–Stokes equations with multiple scales, Journal of Mathematical Analysis and Applications, Volume 464, Issue 2, 15 August 2018, Pages 1408-1424, https://doi.org/10.1016/j.jmaa.2018.04.073
[41] Senjo Shimizu and Hidenobu Tsuritani; On a Navier–Stokes–Ohm problem from plasma physics in multi connected domains, Partial Differential Equations and Applications (2021) 2:75, https://doi.org/10.1007/s42985-021-00122-7

[42] Jean-Luc Cambier and David A. Micheletti, Theoretical Analysis of the Electron Spiral Toroid Concept , NASA/CR-2000-210654, https://ntrs.nasa.gov/api/citations/20010021117/downloads/20010021117.pdf
[43] Sethian J.D, Obenschain S.P, Myers M, Schmitt A.J, Colombant D, Gardner J, Hegler F, Wolford M, Giuliani J, Kepple P., and Swanekamp S; Fusion energy with lasers, direct drive targets, and dry wall chambers; Nuclear Fusion, Volume 43, Number 12; **DOI** 10.1088/0029-5515/43/12/015
[45] Jonas Degrave, Federico Felici, Jonas Buchli, Michael Neunert, Brendan Tracey, Francesco Carpanese, Timo Ewalds, Roland Hafner, Abbas Abdolmaleki, Diego de las Casas, Craig Donner, Leslie Fritz. et al; Magnetic control of tokamak plasmas through deep reinforcement learning. Nature 602, 414–419 (2022). https://doi.org/10.1038/s41586-021-04301-9